

LATVIAN
JOURNAL
of
PHYSICS
and TECHNICAL
SCIENCES

ISSN 0868 - 8257

5

(Vol. 54)

2017

Ind. pasūt. € 1,50
Org. € 15,00

Indekss 2091
Indekss 2092

SATURS

ENERĢĒTIKAS FIZIKĀLĀS UN TEHNISKĀS PROBLĒMAS

Geipele S., Geipele I., Kauškale L., Zeltiņš N., Štaube T., E. Pudzis E. <i>Nanotehnoloģiju un viedo materiālu industrijas attīstība zinātnes un uzņēmējdarbības jomās: Zinātniskie rādītāji. Latvijas pieredze (trešā daļa)</i>	3
Kroičs K., Zaķis J., Suzdaļenko A., Husevs O. <i>GaN transistoru pielietošanas apsvērumi mikroinvertorā enerģijas uzkrājēju integrēšanai maiņstrāvas tīklā</i>	14
Dobrijans R., Vītoliņa S., Lavrinoviča L., Dirba J. <i>Sinhronā reaktīvā dzinēja teorētiskā un eksperimentālā izpēte</i>	26
Čerpinska M., Elmanis-Helmanis R. <i>Hidroagregāta ģenerators dinamiskās gaisa spraugas izmaiņas termiskās izplešanās, centrālās un magnētisko spēku ietekmē</i>	38
Urbahs A., Urbaha M., Carjova K. <i>Vēja enerģētiskās iekārtas planetāra reduktora eksperimentāla prototipa izstrāde un novērtēšana</i>	48
Survilo J. <i>Tīklu pētījumi uz savstarpējo zudumu aprēķinu bāzes</i>	57

ELEKTRONIKA

Pavlovs D., Bobrovs Vj., Parfjonovs M., A. Alševska, Ivanovs Ģ. <i>Signāla reģenerācijas ietekmes novērtēšana uz garās DWDM sistēmas energoefektivitāti</i>	68
--	----

Price to individual subscribers € 1.50/issue
Price to collective subscribers € 15.00/issue

Index 2091
Index 2092

CONTENTS

PHYSICAL AND TECHNICAL ENERGY PROBLEMS

Geipele S., Geipele I., Kaushkale L., Zeltinsh N., Staube T., Pudzis E. <i>The development of nanotechnologies and advanced materials industry in science and entrepreneurship: Scientific indicators. A case study of Latvia (part three)</i>	3
Kroics K., Zakis J., Suzdalenko A., Husev O. <i>Design considerations for GaN-based microinverter for energy storage integration into AC grid</i>	14
Cerpinska M., Elmanis-Helmanis R. <i>Dynamic air gap change of low-speed generator considering thermal expansion, centrifugal force and magnetic force effects</i>	26
Dobriyan R., Vitolina S., Lavrinovicha L., Dirba J. <i>Theoretical and experimental research of synchronous reluctance motor</i>	38
Urbahs A., Urbaha M., Carjova K. <i>Development and assessment of planetary gear unit for experimental prototype of vertical axis wind turbine</i>	48
Survilo J. <i>Grid study on the basis of allocated power loss calculation</i>	57

ELECTRONICS

Pavlovs D., Bobrovs V., Parfjonovs M., Alsevska A., Ivanovs G. <i>Evaluation of signal regeneration impact on the power efficiency of long-haul DWDM systems</i>	68
---	----

Индивид. заказ. € 1,50
Орг. заказ. € 15,00

Индекс 2091
Индекс 2092

СОДЕРЖАНИЕ

ФИЗИКО-ТЕХНИЧЕСКИЕ ПРОБЛЕМЫ ЭНЕРГЕТИКИ

Гейпеле С., Гейпеле И., Каушкале Л., Зелтиныш Н., Штаубе Т., Пудзис Е. <i>Развитие нанотехнологий и передовых материалов в науке и предпринимательстве: научные показатели.</i> <i>Опыт Латвии (часть третья)</i>	3
Кроичс К., Закис Я., Суздаленко А., Хусев О. <i>Рекомендации по использованию GaN транзисторов в микроинвенторах для интеграции энергетических аккумуляторов в сети переменного тока</i>	14
Добриян Р., Витолина С., Лавриновича Л., Дирба Я. <i>Теоретические и экспериментальные исследования реактивного синхронного двигателя</i>	26
Черпинска М., Элманис-Хелманис Р. <i>Динамическое изменение воздушного зазора низкоскоростного генератора с учетом теплового расширения, центробежной силы и магнитного поля</i>	38
Урбахс А., Урбаха М., Царева К. <i>Разработка и оценка экспериментального прототипа планетарного редуктора ветровой турбины</i>	48
Сурвило, И. <i>Сетевые исследования на основе расчета взаимных потерь</i>	57

ЭЛЕКТРОНИКА

Павлов Д., Бобров В., Парфенов М., Алшевска А., Иванов Г. <i>Оценка влияния регенерации сигнала на энергоэффективность дальнемагистральных систем DWDM</i>	68
---	----

LATVIAN
JOURNAL
of
PHYSICS
and TECHNICAL
SCIENCES

LATVIJAS
FIZIKAS
un TEHNISKO
ZINĀTŅU
ŽURNĀLS

ЛАТВИЙСКИЙ
ФИЗИКО-
ТЕХНИЧЕСКИЙ
ЖУРНАЛ

Published six times a year since February 1964
Iznāk sešas reizes gadā kopš 1964. gada februāra
Выходит шесть раз в год с февраля 1964 года

5 (Vol. 54) • **2017**

RĪGA

REDAKCIJAS KOLĒGIJA

I. Oļeņikova (galv. redaktore), A. Ozols, A. Mutule, J. Kalnačs, A. Siliņš,
G. Klāvs, A. Šarakovskis, M. Rutkis, A. Kuzmins, Ē. Birks, S. Ezerniece (atbild.
sekretāre)

KONSULTATĪVĀ PADOME

J. Vilemas (Lietuva), K. Švarcs (Vācija), J. Kapala (Polija), J. Melngailis (ASV),
T. Jēskelainens (Somija), J. Savickis (Latvija), N. Zeltiņš (Latvija), Ā. Žīgurs (Latvija)

EDITORIAL BOARD

I. Oleinikova (Chief Editor), A. Ozols, A. Mutule, J. Kalnacs, A. Silins, G. Klavs, A.
Sarakovskis, M. Rutkis, A. Kuzmins, E. Birks, S. Ezerniece (Managing Editor)

ADVISORY BOARD

Yu. Vilemas (Lithuania), K. Schwartz (Germany), J. Kapala (Poland), J. Melngailis
(USA), T. Jeskelainens (Sweden), J. Savickis (Latvia), N. Zeltinsh (Latvia), A. Zigurs
(Latvia)

Korektore: O. Ivanova
Maketētājs I. Begičevs

INDEKSĒTS (PUBLICĒTS) | INDEXED (PUBLISHED) IN

www.scopus.com

www.degruyter.com

EBSCO (Academic Search Complete, www.epnet.com), INSPEC (www.iee.org.com).

VINITI (www.viniti.ru), Begell House Inc/ (EDC, www.edata-center.com).

Izdevējs: Fizikālās enerģētikas institūts
Reģistrācijas apliecība Nr. 0221
Redakcija: Krīvu iela 11, Rīga, LV-1006
Tel. 67551732, 67558694
e-pasts: ezerniec@edi.lv
Interneta adrese: www.fei-web.lv
Iespiests SIA "AstroPrint"

THE DEVELOPMENT OF NANOTECHNOLOGIES AND ADVANCED
MATERIALS INDUSTRY IN SCIENCE AND ENTREPRENEURSHIP:
SCIENTIFIC INDICATORS. A CASE STUDY OF LATVIA (PART THREE)

S. Geipele¹, I. Geipele¹, L. Kauskale¹, N. Zeltins², T. Staube¹, E. Pudzis¹

¹Institute of Civil Engineering and Real Estate Economics,
Faculty of Engineering Economics and Management,
Riga Technical University,
6-210 Kalnciema Str., LV-1048, Riga, LATVIA

E-mail: Ineta.Geipele@rtu.lv

²Institute of Physical Energetics,
11 Krivu Str., LV-1006, Riga, LATVIA

The present scientific paper is the third part and continuation of the in-depth scientific study of the developed system of engineering economic indicators, where the authors obtain results from the scientific research presented in a series of works on the development of the nanotechnologies and advanced materials industry in science and entrepreneurship in Latvia. Part three determines the crucial scientific indicators of the development of nano-field at the macro, micro, and meso development levels of the economic environment in Latvia. The paper provides the interaction of new identified indicators of nano-field in terms of further scientific and practical activities. Latvia is analysed in comparison with other countries in the world.

Keywords: *advanced materials, development of science, economic environment level, engineering economic indicator system, nanotechnologies, research, scientific indicators*

1. INTRODUCTION

We are at the beginning of a global transformation that is characterised by the convergence of digital, physical, and biological technologies in ways that are changing both the world around us and our very idea of what it means to be human. The Fourth Industrial Revolution is not defined by any particular set of emerging technologies themselves, but rather by the transition to new systems that are being built on the infrastructure of the digital revolution. The fundamental and global nature of this revolution also poses new threats related to the disruptions it may cause – af-

fecting labour markets and the future of work, income inequality, and geopolitical security as well as social value systems and ethical frameworks [1].

In accordance with the above-mentioned topicality and the continuation of the present study, which follows and correlates with the in-depth analysis of the previous two studies [2], [3], the development of the nano-field can also be identified and revealed from the perspective of scientific indicators. With regard to the structure of the research on nanotechnologies and advanced materials industry in science and entrepreneurship, it should be noted that the research will reveal crucial scientific indicators of the development of the nano-field at the macro, micro, and meso development levels of economic environment in Latvia.

The authors have conducted in-depth research on scientific indicators from the perspective of nano-field because they consider that the key aspects determining the competitiveness and productivity of every country are the quality of higher education, skilled labour force, R&D level and development of innovations, which are crucial factors for any economy that follow global trends and modernise simple production processes and create the added value for their products. In the era of innovative technologies and digital revolution, there is also a need for an environment that will foster innovative activities and ideas supported by both the public and private sectors. Investment in R&D is important and necessary, in general, and in the private sector, in particular, where there is an increasing need for high-quality research institutions that can provide the basic knowledge necessary for the development of new technologies, extensive cooperation in research and technological development between universities and the industry. Thus, the development and analysis of scientific indicators at the macro, micro, and meso development levels are topical and relevant.

The **aim** of the research is to develop the scientific indicators at the macro, micro, and meso development levels, evaluate them at the level of Latvia and compare them with the indicators of other countries if applicable to the nano-field in science and entrepreneurship.

To reach the aim of the study – to analyse the scientific indicators characterising the level of development of nano-field in quantitative terms in Latvia, the following research **methods** have been used: statistical, logical, data processing and comparative analysis, the study of the primary and secondary sources of the scientific literature, induction and deduction, scientific overview of theoretical aspects of the issue under consideration, as well as the study of a set of indicators.

The **results** of the research can be used to determine further enhancement of the Latvian nano-field in science and entrepreneurship, and R&D policy, as well as ensure further areas of research.

2. RESULTS AND DISCUSSION

Assessment of the Scientific Indicators

At the macro or global level, the group of scientific indicators includes indicators characterising the development of science, such as the total number of citations

to nano-articles and average citation per nano-article, which are the main indicators evaluating the state's scientific excellence. According to the statistical report by Stat-Nano on the total number of citations to nano-articles, in 2016 Latvia was ranked only 67th out of 105 countries in the world, demonstrating 108 cited nano-articles in compliance with the data of the Web of Science (ISI Web of Knowledge). According to this report, Latvia holds similar positions with Lebanon, Belarus and Jordan [4]. However, in the report on average citation per nano-article, in 2016, Latvia was ranked 53rd out of 106 countries in the world, demonstrating an index of 1.07 that was also achieved by North Korea, the Czech Republic, Lebanon and the UAE [5].

As the next scientific indicator, the authors propose the number and quality of publications and studies by science sectors that indicates the development of scientific productivity and the citation impact of a researcher. To reflect this indicator, the authors use both h-Index of nano-articles according to Web of Science and h-Index in Nanoscience and Nanotechnology according to Scopus and ISI indexed nano-articles. In the report on h-Index of nano-articles according to Web of Science, in 2016 Latvia was ranked 53rd out of 106 countries in the world, obtaining the index of 6.00. Bulgaria, Croatia, Hungary, Luxembourg, Morocco, Nigeria, Norway etc. also demonstrated the same index as Latvia [6]. H-Index in Nanoscience and Nanotechnology according to Scopus shows the following: In 2016, Latvia was ranked 74th out of 131 countries in the world with an h-index of 19, i.e., a number of articles (h) that received at least h citations. Similar indicators were also obtained by Qatar, Indonesia, Luxembourg, Lebanon, Armenia and Venezuela in 2016 [7]. In terms of ISI indexed nano-articles (Web of Science), the authors note that in 2016 Latvia was ranked 68th out of 106 countries with 101 ISI indexed nano-articles. Lebanon, Kazakhstan, and Jordan showed the highest results with regard to this indicator [8]. The analysis of these data and the position of Latvia in the competition of the world's countries demonstrate that the low state funding in R&D, inadequate public and private investment, as well as problems with human resources analysed in the previous two studies are the main factors that hinder the development of scientific research in Latvia.

A more positive trend is observed with respect to the national priority in nanoscience, i.e., the ratio of the total number of nano-articles to the share of articles of the country of the same period. In 2016, by the index of national priority in nanoscience, Latvia was ranked 29th out of 106 countries in the world, by holding the position between Thailand (28th place) and the Czech Republic (30th place). Other countries by the statistical level of a similar indicator are Vietnam, Russia and Taiwan, which have a higher index than Latvia. However, the adjacent countries, according to the lowest ranking, are Bulgaria, Tunisia, Kazakhstan and Azerbaijan. Since 2000, the index of national priority in nanoscience has reached its highest level in 2006, i.e., 2.20. This indicator has been achieved by Latvia, and it is the highest level in statistics of all the above-mentioned countries. In spite of high fluctuations, dynamic changes have been observed in all countries, and at present all these countries, including Latvia, have achieved the index of national priority in nanoscience between 1 and 1.5. This is a decline for Latvia, while Qatar, Egypt, Romania and Vietnam experience high growth [9].

At the global level, it is worth mentioning the number of nano-articles per million people, by which Latvia was ranked 37th in 2016 (51.52 – ratio of nano-

articles to country population (per million people)) out of 106 countries in the world, demonstrating a high growth rate in 2015 and 2016, respectively. However, Cyprus was ranked 36th, while Serbia – 38th. It is interesting to mention the results of the neighbouring countries of Latvia – Estonia was ranked 19th in this rating group, while Lithuania – 33rd [10].

With regard to the group of scientific indicators, the authors have also chosen the share of international collaboration in nanoscience (share of joint nano-articles between one country and other countries, %). In the ranking of 106 countries in the world in 2016, Latvia was ranked 57th with 69.23 %, which compared to 2009 (75 %) means the reduction in the number of international scientific publications in cooperation with foreign authors. Slightly better results were demonstrated in 2016 by Singapore (69.63 %), Bangladesh (69.66 %), Iraq (70.54 %), and slightly lower – by Jordan (68.75 %), Croatia (68.35 %), New Zealand (68.33 %) and France (68.12 %) [11].

As the final scientific indicator at the global level, the number of nano-articles per GDP (article per billion \$) should be mentioned, which shows that Latvia in 2016 was ranked 33rd (1.98 number of nano-articles per billion \$ GDP) out of 106 countries in the world, demonstrating moderate growth rate from 2005 (0.90 number of nano-articles per billion \$ GDP) to 2014 with some fluctuations in the time series. In 2016, slightly better places, i.e., 32nd place and 31st place were taken by Romania and Lithuania, respectively. However, slightly lower positions were occupied by the UK (34th place) and Italy (35th place). It is interesting to note that Estonia was ranked 9th in this ranking [12].

There are a variety of publications concerning nanotechnologies and nanoscience development in general, in oldest and latest publications. For instance, European applications of micro/nanotechnologies were analysed by Antonio Martinez de Aragón (2000) [13], application of nanoscience in construction was analysed by David Tetlow et al. (2017) [14], its environmental applications were analysed by Henning Wigger, Michael Steinfeldt, and Alvis Bianchin (2017) [15] and other scientists. Studies in this area are of high importance. Countries that produce most publications in nanoscience play an important role in the technological development of the country.

At the meso level, the group of scientific indicators includes: the total amount of fundamental studies in materials science per year; persons employed in science and technology; government procurement of advanced technology products; statistics on the creation of new research working groups, which characterise the scientific and research capacity in Latvia at the national level.

In Latvia, fundamental studies related to materials science are mainly carried out by higher education and research institutions, e.g., the University of Latvia, Riga Technical University, as well as separate national research institutes. Several materials science-related centres of excellence, research institutes, laboratories and other academic organisations have also been established, participating in many European and international projects on various topics of materials science. In a number of 27 nano-field programmes from 2002 to 2012 [16], Latvia has participated in 18 scientific projects with a total funding of 30 million EUR, with average EU contribution rate of 77 %. The projects' sum is 30 % larger than one contract value in the USA [17]. It should be noted that in 2016 the Latvian Council of Science funded fundamental

and applied research projects in the amount of 4,388,212 EUR, which amounted to approximately 11 % of the total financing of scientific projects in Latvia [18]. However, according to the Central Statistical Bureau of the Republic of Latvia, in 2015, 152.3 million EUR were invested in research in Latvia, which amounted to 6.5 % less than in 2014. In 2015, foreign funding still made the largest part – 45.0 % – of the total funding in research, 32.7 % was state funding, 20.1 % – private financing, and 2.2 % – university funding. Of the total expenditure on research, the largest part of the expenditure – 67.2 mln. EUR or 44.2 % – was spent on applied research. Total expenditure on fundamental research, compared to 2014, increased by 9.6 %, and in 2015 it amounted to 52.5 mln. EUR [19]. Taking into account that statistical data on projects implemented in Latvia in the field of innovative materials production and high technology industry in the nano-field are difficult to collect and their number may be inaccurate due to a lack of statistics, the authors of the study suggest carrying out a separate study on the level of scientists' awareness about the availability of fundamental research and its evaluation with other European countries.

It is interesting to note that at present strategic plans in nanotechnology development are elaborated and enhanced in countries such as Australia, Austria, Canada, China, Denmark, Finland, Germany, Iran, Ireland, Netherlands, New Zealand, Norway, Pakistan, Poland, Russia, Saudi Arabia, South Africa, South Korea, Switzerland, Thailand, the UK and the USA [20]. For nanoscience development, it should be crucial to develop environmentally-friendly solutions in the development of many industries.

With regard to the next indicator of persons employed in science and technology, the authors state that in the ranking of 28 EU countries in 2016 according to the classification of economic activities – NACE Rev.2 “High-technology sectors (high-technology manufacturing and knowledge-intensive high-technology services)” Latvia was ranked 21st (7.0 % of total employment) and held a similar position with the Netherlands (7.0 %) leaving behind Portugal (6.8 %), Germany (6.3 %), Poland (6.0 %) and other EU countries. It should be noted that the EU average indicator in this category was 7.7 % of total employment. However, in the sample data on persons employed in science and technology “High and medium high-tech manufacturing” in the ranking of 28 EU countries in 2016, Latvia was ranked 25th (2.0 % of total employment), followed by Lithuania (1.4 %), Luxembourg (0.9 %) and Cyprus (0.7 %), while the other EU countries were ranked higher. In this category, the EU average indicator was 5.8 % of total employment [21]. It should also be noted that, according to the data of the Central Statistical Bureau of the Republic of Latvia, in 2016 in Latvia 5,120 employees worked in scientific research according to the full-time equivalent, of which 3,147 – in the higher education sector, 1,077 – in the public sector, and 896 – worked in the business sector [22]. Unfortunately, the authors of the study do not have access to the information on how many people work in the nano-field and business in Latvia. The analysis in this indicator group demonstrates the known problems with human resources, as evidenced by the previously analysed indicators in the groups of economic, social and technical indicators, which show that workers “drain” from the R&D sector due to the lack of motivation compared to other EU countries.

At the meso level, the government procurement of advanced technology products is of importance in the group of scientific indicators. The implementation of

public procurement is essential for the development of both business and public institutions (such as research institutions, centres, incubators, prototype laboratories and experimental facilities). If the results of the procurement contest are appealed, a particular research institution cannot implement the future plans for the implementation of the product or services in a certain project until the decision on the legality of the procurement procedure is made by the Procurement Monitoring Bureau of the Republic of Latvia. To reflect public procurement activities of Latvia in the nano-field, the authors have collected data for the period of 2014–2016 on the results published by the Procurement Monitoring Bureau according to the keyword “nano”, procurement subject and procurement winners. According to the publicly available information of the Procurement Monitoring Bureau, within this period 32 procurements were made in the nano-field in Latvia, of which 8 winners were research institutes (Ventspils University College, the University of Daugavpils, Riga Stradins University, the University of Latvia, Riga Technical University, Agency of the University of Latvia “Institute of Physics of the University of Latvia”, Latvian State Institute of Wood Chemistry and state research institute – derived public entity “Institute of Electronics and Computer Science”), one winner – commercial company POLYMERS Ltd. and autonomous body governed by public law – Public Utilities Commission [23]. It should also be noted that according to the Global Competitiveness Report 2016–2017, Latvia was ranked 98th out of 138 countries in the world [1] by the indicator characterising innovation – government procurement of advanced technology products –, which shows that there is not enough public funding in innovation development that is also confirmed by public funding in R&D analysed in previous studies, low indicator of university-industry collaboration in R&D, human resources and other issues.

As the final indicator in this group at the meso level, the authors have included statistics on the creation of new research working group, which means that in 2014 10 working groups were established in Latvia within the framework of the EU Structural Funds [24]. The latest statistical data are not available to the authors of the study, as well as comparative statistical information on other countries.

At the same time, the authors also acknowledge that the indicators proposed at the meso level deserve deeper study in order to assess the potential and find conceptual solutions to R&D activities by determining science and technology strategies at the national level in the future.

At the micro or enterprise level, the authors put forward the following indicators in the group of scientific indicators: the number of start-up companies in alliance with universities and valorisation indicators, as well as ratio of employees involved in research and innovation activities.

The number of people employed in science, research, technological development and innovation is too small in Latvia, as well as there is insufficient renewal of the personnel involved in these areas and limited funding. The research, technological development and especially innovation infrastructure are underdeveloped. As a result, there is a small number of spin offs and start-up companies based on developments in the public research sector [25]. According to the Global Competitiveness Report 2016–2017, Latvia has been ranked 99th out of 138 countries in the world by the availability of scientists and engineers [1], which also justifies and complements

the previously analysed information. The afore-mentioned problem proves that the disproportionately low proportion of basic funding in R&D does not contribute to a strategic and science-intensive development of the country and, accordingly, entrepreneurship in Latvia.

Start-up companies and the valorisation process in the area of nanotechnologies are of high scientific and practical significance. Currently, the studies and statistical development tendencies show that both the higher education sector and the business sector receive investments in R&D. The analysis [26] shows that some universities actively participate in valorisation, business incubator creation, establish innovative centres and perform other activities [27], [28]. The loans issued from banks to non-bank institutions to professional, scientific and technical services in Latvia in 2017Q2 are one of the lowest; however, the activities of enterprises in the nano-field can be integrated into construction, after supply and waste management and other areas as well [29]. According to the public information available at the Labs of Latvia – a start-up community platform, the problems of Latvian tech start-up ecosystem are the following: insufficient external networking, lack of smart money, weak deal flow, funding gap, technical skills and knowledge, unique ideas, entrepreneurial skillset etc. [30].

Despite the fact that according to the Global Competitiveness Report 2016–2017 Latvia ranked only 96th out of 138 countries in the world by the market size with relatively small population and other previously described problems, as well as taking into account the transition of Latvia from the efficiency-driven stage to innovation-driven stage [1], Latvia can boast of five start-ups in the nano-field – Catalyco (early stage), Naco Technologies (existed), Nano 55 (early stage), Nano RAY-T (early stage) NanoOptoMetrics (early stage) [30]. Despite the problems encountered in science, business development and cooperation in the nano-field in Latvia, the authors believe that, according to the experience and fundamental research carried out by Latvian research institutes and enterprises, Latvia has untapped potential for improving existing materials, production, technology methods and developing new innovations in high-technology and the medium-high-technology industry, which determines the efficient use of products in a particular economic sector, promotes the development of science-intensive production and interdisciplinarity of research.

The final scientific indicator at the micro level is the ratio of employees involved in research and innovation activities that illustrates the ratio of employees working in research (see at the meso level) to those working in the field of innovation. Unfortunately, data on employment in the field of innovation are not made public. Taking into account the position of Latvia among other countries in the world by the pillars of labour market efficiency, business sophistication and innovation of the Global Competitiveness Report 2016–2017 [1], the innovative performance of Latvia in the development of the nanotechnology and smart materials industry is still at the developing stage, which is influenced by the factors analysed above.

Referring to the previous research on scientific indicators at all levels, it can be concluded that the indicators characterising the development of scientific research are closely related to the amount of funding allocated to the research activity (see assessment in the group of economic indicators [2]) and the number of people employed in science. Although the scientific development indicators of Latvia in comparison with other countries of the world are average, the performance of scientific

development indicators actually corresponds to the amount of financing invested in science and even would be higher if public funding in R&D were at the level of developed countries of the EU. Despite the problems encountered in the development of Latvian science, in general, science in Latvia is considered to be sufficiently active and innovation-driven, although it is at the developing stage. Thus, the analysis of the indicators characterising the development of the scientific environment indicates the potential for research development, directions for attracting investment and the need for state funding in order to find conceptual solutions, increase competitiveness and potential opportunities for improving the performance of the research and innovation environment.

3. CONCLUSION

1. Within the framework of the development of the system of engineering economic indicators, scientific indicators have been identified at the macro, micro, and meso development levels and assessed at the level of Latvia and compared with those of other countries in the world, if applicable to the nano-field in science and entrepreneurship.
2. The analytical assessment of scientific indicators substantiates and can indicate the competitiveness and productivity of each country, as well as in the age of new technologies and digital revolution highlights the importance of high quality higher education, skilled labour force, R&D level and innovation development for any economy. High-quality research institutions can create fundamental knowledge necessary for the development of new technologies, while universities in cooperation with the industry can modernise simple production processes and create additional added value for existing products.
3. In the field of nanotechnologies and nanoscience at the macro development level, the level of scientific excellence and the development of its productivity in a particular economy can be assessed using the following indicators: the total number of citations to nano-articles; average citation per nano-article; number and quality of publications and studies by science sectors; national priority in nanoscience; number of nano-articles per million people; share of international cooperation in nanoscience; number of nano-articles per GDP. The analysis and comparison of these indicators with other countries of the world indicate that the development and performance of Latvia in this group of scientific indicators is considered average, and there are still factors hindering the development of scientific research in Latvia.
4. The scientific indicators analysed at the meso level describe the national (Latvia's) level of science and research capacity and provide data for the promotion of the national development in accordance with the extent of nano-industry and science development at the local level. It should be noted that in this group of indicators, the authors have encountered the lack of availability of data on projects implemented in Latvia in the field of innovative materials production and high technology in the nano-field,

number of employees in the field of nanoscience and entrepreneurship, as well as the lack of current statistics on the creation of new scientific research working groups. Based on publicly available information, the analysis demonstrates the ongoing human resource problems in Latvia. According to the assessment performed and the findings revealed in this discipline, the authors propose that the evaluation of the effectiveness of fundamental and applied research projects in specific sectors of the national economy should be ensured at the national (Latvia's) level.

5. A disproportionately low proportion of base financing in R&D does not contribute to strategic and science-intensive development and entrepreneurship in Latvia. Thus, the indicators identified at the micro level demonstrate the capacities of the domestic producers, the capital capacity of entrepreneurs and the degree of readiness for the development and use of the next generation of nano-technologies.
6. The analysis of the conducted research, its main results and the conclusions formulated substantiate the need to continue the research on the development possibilities of nanotechnologies and advanced materials industries in science and entrepreneurship in Latvia in several directions, by reducing the factors hindering the development of scientific research in Latvia, envisaging environmentally-friendly solutions in the development of many industries and promoting the development of science-intensive production, as well as ensuring interdisciplinarity of research.

REFERENCES

1. Schwab, K. (2016). *The Global Competitiveness Report 2016–2017*. World Economic Forum. Retrieved from <https://www.weforum.org/reports/the-global-competitiveness-report-2016-2017-1>
2. Geipele, I., Geipele, S., Štaube, T., Ciemleja, G., & Zeltniš, N. (2016). The development of nanotechnologies and advanced materials industry in science and entrepreneurship: Socioeconomic and technical indicators: A case study of Latvia (Part One). *Latvian Journal of Physics and Technical Sciences*, 53(4), 3–13. ISSN 0868-8257. Available at doi:10.1515/lpts-2016-0023
3. Geipele, I., Geipele, S., Štaube, T., Ciemleja, G., & Zeltniš, N. (2016). The development of nanotechnologies and advanced materials industry in science and entrepreneurship: socioeconomic and technical indicators. A case study of Latvia (Part Two). *Latvian Journal of Physics and Technical Sciences*, 53(5), 31–42. ISSN 0868-8257. Available at doi: 10.1515/lpts-2016-0034
4. StatNano. (n.d.). *Total number of citations to nano-articles (Citation)*. Retrieved from <http://statnano.com/report/s36>
5. StatNano. (n.d.). *Average citation per nano-article (citation per article)*. Retrieved from <http://statnano.com/report/s55>
6. StatNano. (n.d.). *H-Index of nano-articles..* Retrieved from <http://statnano.com/report/s38>
7. SCImago Journal & Country Rank. (n.d.). *Country Rankings*. Retrieved from <http://www.scimagojr.com/countryrank.php?category=2509&year=2016>

8. StatNano. (n.d.). *ISI indexed nano-articles (Article)*. Retrieved from <http://statnano.com/report/s29>
9. StatNano. (n.d.). *National priority in nanoscience*. Retrieved from <http://statnano.com/report/s41>
10. StatNano. (n.d.). *Number of nano-articles per million people (Article per million people)*. Retrieved from <http://statnano.com/report/s33>
11. StatNano. (n.d.). *Share of international collaboration in nanoscience generation (Percent)*. Retrieved from <http://statnano.com/report/s82>
12. StatNano. (n.d.). *Number of nano-articles per GDP(ppp) (Article per billion \$)*. Retrieved from <http://statnano.com/report/s81>
13. De Aragón, A. M. (2000). European applications of micro/nano-technologies to space ESA overview. *IFAC Proceedings*, 33(26), 315–320. [https://doi.org/10.1016/S1474-6670\(17\)39163-2](https://doi.org/10.1016/S1474-6670(17)39163-2)
14. Tetlow, D., De Simon, L., Liew, S. Y., Hewakandamby, B., Mack, D., Thielemans, W., & Riffat, S. (2017). Cellulosic-crystals as a fumed-silica substitute in vacuum insulated panel technology used in building construction and retrofit applications. *Energy and Buildings*. <http://dx.doi.org/10.1016/j.enbuild.2017.08.058>
15. Wigger, H., Steinfeldt, M. & Bianchin, A. (2017). Environmental benefits of coatings based on nano-tungsten-carbide cobalt ceramics. *Journal of Cleaner Production*, 148, 212–222. <http://dx.doi.org/10.1016/j.jclepro.2017.01.179> 0959-6526
16. Maghrebi, M., Abbasi, A., & Amiri, S. (2011). A collective and abridged lexical query for delineation of nanotechnology publications. *Scientometrics*, 86(1), 15–25.
17. Staube, T., Ciemleja, G., & Geipele, I. (2014). Nanoscience: The scale of Latvia. *Advanced Materials Research, 1004–1005: Advanced Materials and Technologies*. Chapter 1: Nano Materials Science and Technology. Edited by Xianghua Liu. - Trans Tech Publications Inc., Durnten-Zurich, Switzerland, 2014, pp. 28–31. ISSN: 10226680. ISBN: 978-303785601-7. DOI: 10.4028/www.scientific.net/AMR.1004-1005.28
18. Latvian Council of Science. (2016). *Fundamental and applied research projects funded by the Latvian Council of Science in 2016..* Retrieved from <http://www.lzp.gov.lv/parskati/Fin-2016.htm>
19. Central Statistical Bureau of Latvia. (2016). *Research Statistics 2016*. Retrieved from http://www.csb.gov.lv/sites/default/files/publikacijas/2016/nr_36_petniecibas_statistika_16_00_lv.pdf
20. StatNano. (2017a). *Strategic Plans*. Retrieved from <http://statnano.com/strategicplans>
21. Eurostat Statistics. (n.d.). *Employed HRST by category, age and NACE Rev. 2 activity (from 2008 onwards)*. Retrieved from <http://appsso.eurostat.ec.europa.eu/nui/submit-ViewTableAction.do>
22. Central Statistical Bureau of Latvia. (n.d.). *Number of employees in scientific research work*. Retrieved from http://data.csb.gov.lv/pxweb/lv/zin/zin_zin/ZI0020.px/table/tableViewLayout2/?rxid=cdeb978c-22b0-416a-aacc-aa650d3e2ce0
23. Procurement Monitoring Bureau of the Republic of Latvia. (n.d.) *Search for announcements*. Retrieved from <http://iub.gov.lv/lv>
24. EU Structural Funds in Education and Science. (n.d.). *The second round of project selection announced in ESF activity 1.1.1.2 “Involvement of Human Resources in Science”*. Retrieved from http://esfondi.izm.gov.lv/1_1_1_2_aktivitates_2_projektu_iesniegumu_atlases_karta
25. Cabinet of Ministers. (2013). *Informative Report “Guidelines for Science, Technology Development and Innovation 2014–2020”*. Decree No.685 of the Cabinet of Ministers as of 28 December 2013.

26. Eurostat. (n.d.). *Total intramural R&D expenditure (GERD) by sectors of performance in Latvia, total (2000 – 2015)*. Database. Retrieved from <http://ec.europa.eu/eurostat/data/database>
27. RTU. (n.d.) Valorization. Retrieved from <https://www.rtu.lv/en/valorization>
28. LU. (n.d.) Innovation Centres and Incubators. Retrieved from <http://www.lu.lv/par/strukt/departamenti/zinatniskas-darbibas-un-projektu-departaments/ic/pieejamais-atbalsts/citas-organizacijas/inovaciju-centri-un-inkubatori/>
29. Financial and Credit Market Commission. (2017). *Credit Institutions. Bank Activities in Latvia in 2017Q2*. Appendix 5. FKTK. Retrieved from <http://www.fktk.lv/en/statistics/credit-institutions/quarterly-reports.html>
30. Labs of Latvia. (n.d.) *Start-up*. Retrieved from <http://www.labsoflatvia.com/lv/start-up->

NANOTEHNOLOĢIJU UN VIEDO MATERIĀLU INDUSTRIJAS ATTĪSTĪBA ZINĀTNES UN UZŅĒMĒJDARBĪBAS JOMĀS: ZINĀTNISKIE RĀDĪTĀJI. LATVIJAS PIEREDZE (TREŠĀ DAĻA)

S. Geipele, I. Geipele, L. Kauskale, N. Zeltins, T. Staube, E. Pudzis

Kopsavilkums

Dotais zinātniskais pētījums ir turpinājums jau diviem nopublicētajiem pētījumiem par padziļinātu un atsevišķu inženierekonomisko rādītāju sistēmas grupu izpēti, kurā autori apkopo zinātniskā pētījuma gaitā iegūtos rezultātus nanotehnoloģiju un viedo materiālu industrijas attīstības līmeņa noteikšanai un paaugstināšanai zinātnē un uzņēmējdarbības jomā Latvijā. Pētījums ietver zinātnisko rādītāju izvērtējumu Latvijas makro, mezo un mikro ekonomiskās vides attīstības līmeņos, kā arī izstrādāto zinātnisko rādītāju salīdzinājumu ar pasaules, tai skaitā Eiropas, valstīm, ja dati bija pieejami. Pētījuma rezultāti norāda uz zinātnisko rādītāju aktualitāti un potenciālu, ja tiks atrisinātas pētījumā konstatētās problēmas.

20.09.2017.

DESIGN CONSIDERATIONS FOR GAN-BASED MICROINVERTER FOR
ENERGY STORAGE INTEGRATION INTO AC GRIDK. Kroics^{1,2}, J. Zakis², A. Suzdalenko², O. Husev²¹Institute of Physical Energetics
11 Krivu Str., Riga, LV-1006, LATVIA
e-mail: kaspars.kroics@gmail.com²Riga Technical University
1 Kalku Str., Riga, LV-1658, LATVIA
e-mail: janis.zakis@rtu.lv

A full bridge converter with electrolytic capacitor on the dc bus is a widely used approach for a single phase interface for renewable energy source generation or energy storage integration in the utility grid. New wide bandgap devices enable higher switching frequency, higher efficiency and higher power density. In the paper, the authors introduce the challenges associated with an increase in switching frequency of a single phase inverter and implementation of wide bandgap GaN-based transistors instead of traditional Si-based transistors. The low gate threshold voltage of GaN transistor and unique reverse conduction behaviour require different driving circuit. The design of the driver circuit and other practical issues are analysed in the paper. The paper also presents some practical results. The research results can be useful to avoid mistakes by designing GaN-based power converters as these devices become increasingly interesting for commercial applications.

Keywords: *energy storage, GaN transistor, high frequency power converter, microinverter, wide bandgap devices*

1. INTRODUCTION

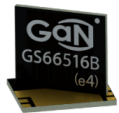

Wide bandgap (WBG) semiconductors such as Silicon Carbide (SiC) and Gallium Nitride (GaN) provide advantages over conventional Silicon (Si) power devices, as shown in Fig. 1. Higher breakdown field of a WBG semiconductor allows for devices to be optimised with thinner drift regions, resulting in power devices with lower specific on-resistance [1]. High electron mobility of GaN allows reducing on-resistance of transistors. This allows achieving high current capability with smaller die; therefore, input and output capacitances are lower than in the case of Si transistors (Table 1). Lower capacitance means that faster switching on and off is possible. Material properties of GaN semiconductors result in a device with lower

on-resistance and switching losses than a Si-based semiconductor with comparable voltage and current capabilities.

In high power density and high efficiency power electronics applications with power ratings around several kilowatts, wide bandgap semiconductors are progressively replacing Si MOSFETs [2] due to the improved switching performance and lower switching losses. The comparison of the main parameters of GaN transistor GS66516B and Si IPT65R033G7 is given in Table 1; the data are taken from the on-line electronic part catalogue (www.mouser.com). Both semiconductors have quite similar breakdown voltages and nominal current; therefore, other parameters should also be analysed in order to choose the transistor that is appropriate for implementation in the switching converter. Si-based transistors have significantly larger output capacitance and bad reverse recovery behaviour of the body diode. In contrast, GaN semiconductors feature much smaller output capacitance and do not suffer from reverse recovery, thus allowing one to achieve higher efficiency, especially, at high switching frequency and in hard switching topologies. The main reason why GaN transistors are not widely used is a significantly higher price and a lack of knowledge of engineers about the right schematic, layout design, EMI, passive component selection and calculation for higher frequencies, etc. to get benefit from using GaN transistors.

Table 1

Comparison of GaN and Si-Based Transistors

Symbol			Value	Parameter
	GS66516B	IPT65R033G7		transistor
V_{DS}	650	700	V	drain source voltage
$R_{DS(on)}, T_J=25^{\circ}C$	25	29	m Ω	drain to source on resistance
$R_{DS(on)}, T_J=150^{\circ}C$	65	72	m Ω	drain to source on resistance
$V_{GS(th)}$	1.3	3.5	V	gate to source voltage threshold
$V_{GS(max)}$	-10 ... +7	-20 ... +20	V	maximum gate to source voltage
C_{ISS}	500	5000	pF	input capacitance
Q_G	12.1	110	nC	total gate charge
Q_{GD}	3.4	35	nC	gate to drain charge
Q_{GS}	4.4	27	nC	gate to source charge
Q_{RR}	0	9	μ C	reverse recovery charge
	40	13	€	price

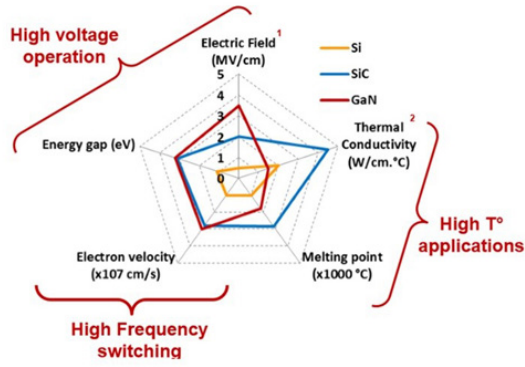


Fig. 1. Comparison of different types of transistor materials [3].

2. GATE DRIVER DESIGN

As can be seen in Table 1, GaN transistors typically come with much lower gate charge Q_G compared to similarly rated Si MOSFETs. Therefore, GaN semiconductors are a promising way to increase the switching frequency without suffering high additional power losses. The gate control of GaN transistors significantly differs from typical silicon Si MOSFETs. One of the main differences in terms of gate control is the gate threshold voltage $V_{GS(th)}$, the gate plateau and the maximum gate voltage $V_{GS(max)}$. As can be seen in Table 1, the maximum gate voltage V_{GS} is much lower than in Si MOSFETs, but anyway most GaN FETs are not fully turned on until V_{GS} reaches about 4 V [4]. To turn off the GaN transistor, the gate voltage must be kept below the minimum gate threshold voltage, which is 1.3 V in this case. This can be a challenge in topologies where the GaN semiconductor drain is exposed to a high dv/dt or the GaN transistor can be switched on from the EMI voltage spikes on the gate.

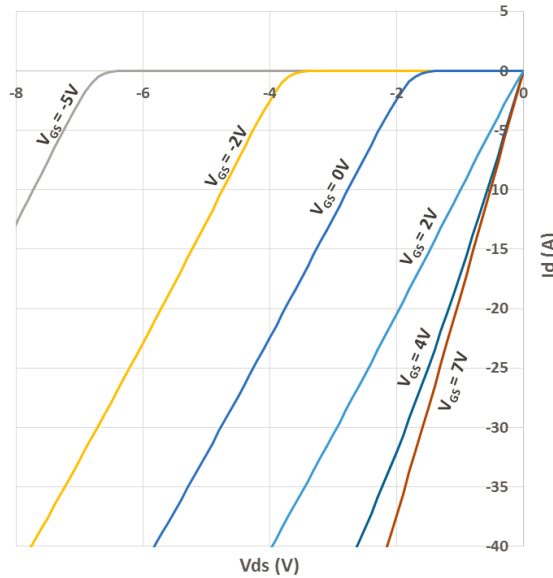


Fig. 2. GaN transistor GS66508P reverse bias characteristics [5].

To increase driver circuit stability against EMI and to increase dv/dt immunity, negative V_{GS} can be applied when the transistor is in off state. The enhancement-mode GaN transistors have specific behaviour: they do not have internal body diode but when the gate is turned off and drain is negative with respect to source, the GaN transistor conducts current from source to drain. The reverse bias characteristics of GaN transistor can be seen in Fig. 2. Applying a negative gate voltage to the transistor increases the voltage drop between source and drain during dead-time conduction. This voltage drop decreases efficiency of the converter; therefore, large negative voltage is not desirable. Even with precise dead-timing, the large voltage drop from drain to source still results in a significant variation of the bootstrap voltage [4]; therefore, bootstrap voltage source for driver is not preferable in this case.

Larger forward voltage drop of GaN transistors compared to MOSFETs during dead-time conduction produces additional power losses. Manufacturers of GaN semiconductors advise short dead-timing control to improve efficiency or add external anti-parallel fast Schottky diode [6]. Loss measurements have been carried out for switching converter with a negative gate voltage of GaN transistors in [7], [8]. Usually, in the scientific papers a gate drive which keeps the device turned off by applying zero volt to the gate to reduce losses during dead time, but for high frequency switching converter such design cannot be suitable as the energy stored in the parasitic loop inductance and the dv/dt stress are high. In the present paper, an approach to use -3V negative gate voltage $V_{GS(off)}$ is demonstrated in order to increase reliability of the converter despite the fact that there will be additional power losses. As can be seen in Table 1, there are no reverse recovery losses during switching; therefore, the required dead time is short.

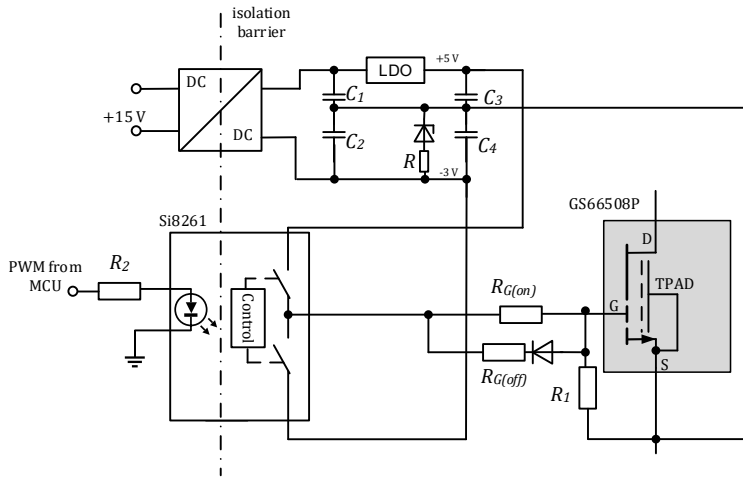


Fig. 3. The schematic of the developed driver.

There are only a few gate driver integrated circuits on the market that fit the requirements of GaN transistors. The LM5113 is a good solution for GaN transistors in applications below 100 V. Silicon Labs produces isolated gate driver integrated circuits that are suitable for GaN devices, compatible with voltages in the kV range. The digital isolation in these drivers is based on radio frequency; therefore, driver

has high common-mode transient immunity. Although common-mode transient immunity of driver is high, the printed circuit board should be designed very carefully to limit stray inductances and capacitances.

Figure 3 shows schematic of the driver circuit. As gate driver Si8261 integrated circuit is used, isolated DC-DC converter is used as power supply for both low side and high side driver circuits because in the case of non-isolated gate driver gate current flows through parasitic inductance L_s (Fig. 4) causing grounding problems. To protect gate from voltage spikes above threshold or maximum rating Zener diodes should be applied between G and S terminals, pull down resistor R_1 equal to $10\text{ k}\Omega$ should be connected to prevent false turn on. Gate resistors with $R_{G(\text{on})} = 10\text{ }\Omega$ and $R_{G(\text{off})} = 5\text{ }\Omega$ are used for turn-on and turn-off processes. If zero voltage is used to turn off, the transistor diode with low voltage drop should be used to provide successful turn off of the transistor.

Gate drive impedance (R_G and L_G) is critical for turn off; therefore, the gate needs to be held down as strong as possible with minimum impedance. Miller effect is more prominent at 650V than 100V design due to higher dv/dt . The equivalent circuit during turn off of the transistor is shown in Fig. 4. To minimise parasitic gate inductance, the driver should be placed as close as possible to the transistor gate. As GaN transistors have extremely low Q_G and drive loss 0603 SMD resistors can be used and driver placed near the gate. Gate resistor allows determining switching speed. High value of $R_{G(\text{on})}$ slows down switching and increases loss, whereas too small $R_{G(\text{on})}$ leads to high dv/dt that can cause gate oscillations and additional losses. High dv/dt causes high common mode currents; therefore, it is important to minimise coupling capacitances of isolated power supply and use a gate driver with high common mode transient immunity.

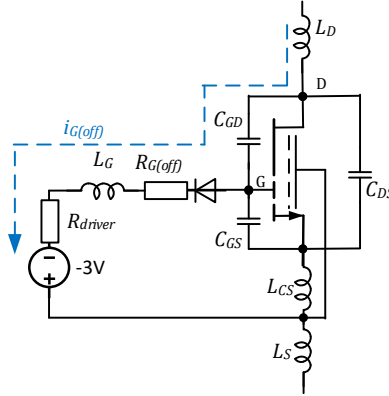


Fig. 4. The equivalent circuit of GaN transistor with a driver during turning off.

3. THE EXPERIMENTAL PROTOTYPE

In order to test the performance of 650 V GaN transistors, a full bridge inverter with LC filter has been designed (Fig. 5). The converter consists of four GS66508P GaN transistors. These transistors have package with low inductance of inner con-

nections, the device is bottom side cooled, so the thermal vias should be introduced into PCB and heat sink placed from the opposite side of the PCB; the proper cooling design is described in [9].

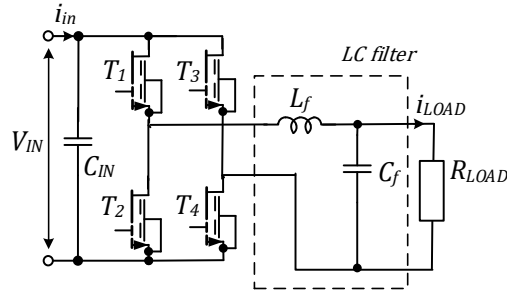


Fig. 5. AC single phase inverter with GaN transistors.

Figure 6 shows a photo of GaN-based inverter prototype; capacitive leg of the full bridge inverter consist of 1 mF electrolytic capacitor and additional ceramic capacitors close to the connection to the transistors. The PCB is intended to extend inverter functionality with a possibility to integrate renewable energy source and energy storage by using single stage quasi Z source topology that is analysed in [10]–[12]. The radiator is placed on the opposite side of the PCB. For the control of the inverter STM32F4 microcontroller was used. For measurement of the current the PCB was extended with a wire to be able to impose oscilloscope current clamp. This additional parasitic inductance introduced significant current ripple; therefore, this loop was removed.

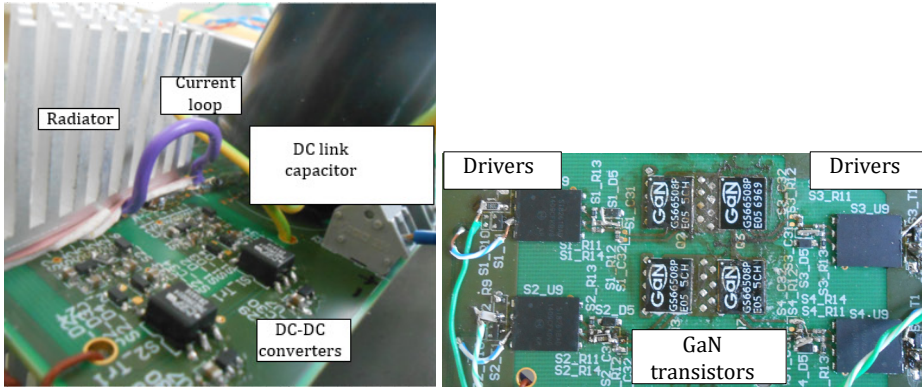


Fig. 6. Photo of the experimental prototype: top side and bottom side of the PCB.

The measurement of the signals of the high frequency GaN power converter is really challenging because any measurement has some impact on measurement results. Some measurement solutions are given in [13], one of the methods to avoid impact on the operation of the converter is to use the calorimetric measurement method. The performance of GaN transistor by using a calorimetric method is measured in [14], [15]. The simple temperature measurement (Fig. 7) via a thermal imaging camera was used to make a relative assessment of efficiency improvement or decrease by changing parameters.

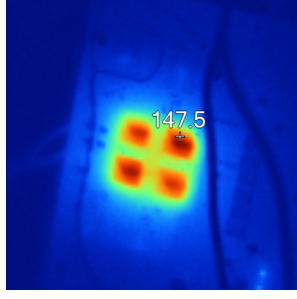


Fig. 7. Thermal image of GaN transistors (temperature in Fahrenheit).

4. THE EXPERIMENTAL RESULTS AND DISCUSSION

As can be seen in Fig. 2, in reverse conduction region the losses are significant; therefore all of the traditional modulation methods (unipolar, asymmetrical unipolar, bipolar) but with using of synchronous rectification and for efficiency improvement dead time should be as short as possible. For hard switching dead time set in PWM from a microcontroller should be larger than the worst-case propagation delay difference plus gate turn on and turn off delay difference that is typically equal to ± 5 ns [16] and varies with the value of R_G . Figure 8 shows driver input and output signals. Driver turn on delay is equal to 40 ns but turn off delay is equal to 30 ns and this corresponds to the information in Si8261 datasheet [17]. In [17] the worst-case propagation delay is given and it is equal to 25 ns. It means that for practical applications the dead time must be set larger than 30ns and plus some safety margin. In the scientific papers for 650 V GaN transistors dead time is usually in the range from 40 to 120 ns and this is mainly determined by the driver delay.

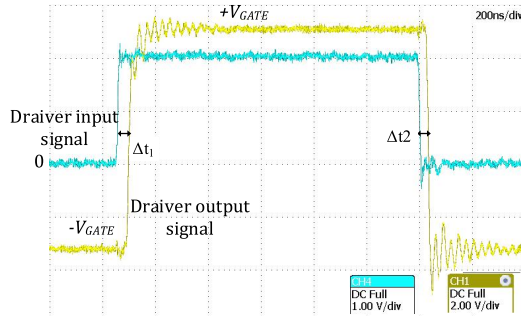


Fig. 8. Oscillogram of the driver input and output signals.

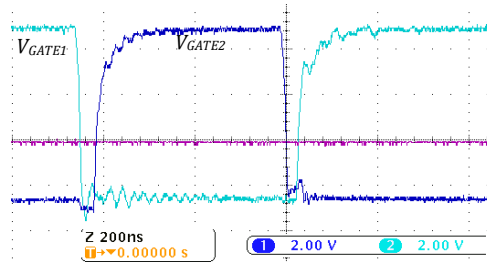


Fig. 9. Signals to the gate with inserted dead time, $R_{G(on)} = 30 \Omega$.

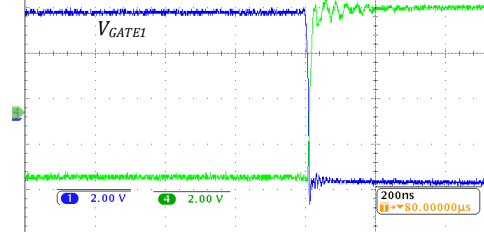


Fig. 10. Signals to the gate with small dead time, $R_{G(on)} = 10 \Omega$.

As can be seen in Figs. 9 and 10, the gate resistor determines how fast gate capacitance is charged and how fast GaN transistor is switched on and off. As can be seen in Figs. 9 and 10, 30Ω does not allow using all benefits from fast switching of GaN transistor and switching losses will be high. Too small gate resistor can lead to high dv/dt that causes EMI problems. In this case, gate resistance is selected equal to 10Ω as compromise between both cases.

The dead time was changed and temperature of GaN transistors was measured to determine the most efficient dead time. Although these measurements give only a very approximate idea about losses, they can provide a comparative analysis. As the difference between driver turn off and turn on delays is equal to 10 ns (Fig. 8), the most efficient dead time generated from a microcontroller in temperature measurements is 0 ns since the dead time equal to 10 ns will be on the driver output (Fig. 10) due to driver delay and this dead time is enough for GaN transistor switching transitions. The impact of dead time on the efficiency of GaN transistors is also analysed in [4], [6], [7], [16]. In the literature, it is proposed to use 0 ns dead time for switching on and about 30 ns dead time for switching off, but the analysis is provided for driver with 0 V turn off voltage. Different turn off and turn on dead time is more complicated to implement as in microcontrollers there is usually no such a choice to set different dead time. Optimal dead time also varies depending on current, duty cycle and other parameters; therefore, the selection of optimal dead time is a complicated task, especially, in inverter as the current varies during the time. In practical applications, the worst-case driver delay difference should be taken into account and dead time should be at least 30 ns .

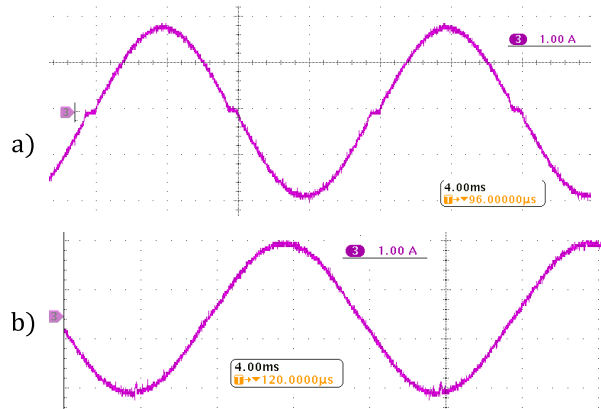


Fig. 11. Oscillogram of the load current a) with 170 kHz and small dead time; b) with 350 kHz and higher dead time.

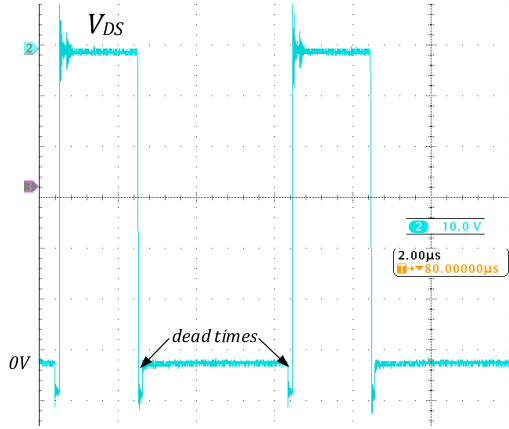


Fig. 12. Oscillogram of drain to source voltage.

Figure 11 shows waveforms of output current. The inverter is tested in the open loop condition without any feedback. The temperature measured during an increase in switching frequency shows a decrease in efficiency. The results of Little Box Challenge show that optimal frequency that reduces volume of passive components but does not significantly increase volume of heatsink is in the range from 80 to 200 kHz [18]. The dead time also influences waveform of the output sinusoidal signal as can be seen in Fig. 11b. If the working frequency is high, the high performance microcontroller or FPGA is needed to generate PWM with high resolution.

Figure 12 shows a waveform of drain-to-source voltage during the switching operation. Very high dv/dt can be achieved by using GaN transistors. In this case, 10 Ω gate resistor was used but this value could be reduced to increase dv/dt even more. The challenge is to design proper PCB to deal with such high dv/dt and di/dt . The first prototype had a few mistakes that did not allow increasing dv/dt and produced some EMI issues. Design of the converter with tight loop and low parasitic inductances is very important to get full benefit from GaN transistor applications.

5. CONCLUSIONS

The practical implementation of GaN transistors needs new knowledge, especially, in high frequency applications. Due to fast transients, decoupling of the voltage bus has to be done with minimal loop inductance; therefore, the current measurement through transistor can be challenging and calorimetric measurement methods can be applied. GaN transistor has no body diode but the channel reverse conduction is possible when gate voltage is below threshold voltage. Using 0V voltage to turn off is the simplest solution that limits power losses during dead time, but such gate voltage does not ensure sufficient safety against the false turn on and limits maximum dv/dt . Using negative voltage during turn off produces additional losses during dead time, the optimum of dead time is complicated to find and mainly minimum dead time is determined by the worst-case delay differences of driver circuit. The value of the gate resistor determines switching speed – a value less than 10 Ω allows increasing dv/dt , but losses in the gate capacitance increase and high dv/dt requires proper design of the converter.

ACKNOWLEDGEMENTS

The present research has been supported by the Latvian National Research Programme “LATENERGI” and the Latvian Council of Science (Grant 673/2014).

REFERENCES

1. Jones, E. A., Wang F. F., & Costinett, D. (2016). Review of Commercial GaN Power Devices and GaN-Based Converter Design Challenges. *IEEE Journal of Emerging and Selected Topics in Power Electronics*, 4(3), 707–719.
2. Bortis, D., Knecht, O., Neumayr, D., & Kolar, J. W. (2016). Comprehensive evaluation of GaN GIT in low- and high-frequency bridge leg applications. In *IEEE 8th International Power Electronics and Motion Control Conference*, 22–25 May 2016 (pp. 21–30). Hefei, China.
3. Rise of the 3rd Generation Semiconductor Silicon Carbide Technology. [Online]. Available at <http://www.iabrasive.com/articles/rise-of-the-3rd-generation-semiconductor-silicon-carbide-technology>. [Accessed: 04-Aug-2017].
4. Roschatt, P. M., McMahon, R. A., & Pickering, S. (2015). Investigation of dead-time behaviour in GaN DC-DC buck converter with a negative gate voltage. In *9th International Conference on Power Electronics and ECCE Asia*, 1–5 June 2015 (pp. 1047–1052). Seoul, Korea.
5. Sørensen, C., Lindblad Fogsgaard, M., Christiansen, M. N., Kjeldal Graungaard, M., Nørgaard, J. B., Uhrenfeldt, C., & Trintis, I. (2015). Conduction, reverse conduction and switching characteristics of GaN E-HEMT. In *2015 IEEE 6th International Symposium on Power Electronics for Distributed Generation Systems (PEDG)*, 22–25 June 2015 (pp. 1–7). Aachen, Germany: IEEE Press.
6. Strydom, J., & Reusch, D. (2013). Dead-time optimization for maximum efficiency. *Efficient Power Conversion (EPC) Whitepaper*.
7. Hoffmann, L., Gautier, C., Lefebvre, S. & Costa, F. (2014). Optimization of the Driver of GaN Power Transistors through Measurement of Their Thermal Behavior. *IEEE Transactions on Power Electronics*, 29(5), 2359–2366.
8. Chub, A., Zdanowski, M., Blinov A., & Rabkowski, J. (2016). Evaluation of GaN HEMTs for high-voltage stage of isolated DC-DC converters. In *10th International Conference on Compatibility, Power Electronics and Power Engineering*, 29 June–1 July 2016 (pp. 375–379). IEEE.
9. PCB Thermal Design Guide for GaN Enhancement Mode Power Transistors. [Online]. Available at http://www.ecomal.com/fileadmin/Datenblaetter/GaN_Systems/App_Notes/GN005_App_Note-PCB_Thermal_Design_Guide_for_GaN_Enhancement_Mode_Power_Transistors.pdf [Accessed: 06-Aug-2017].
10. Matiushkin, O., Husev, O., Tytelmaier, K., Kroics, K., Veligorskyi, O., & Zakis, J. (2017). Comparative analysis of qZS-based bidirectional dc-dc converter for storage energy application. In *Technological Innovation for Smart Systems*, 3–5 May 2017 (pp. 409–418). Costa de Caparica, Portugal.
11. Kroics, K., Zakis, J., & Husev, O. (2017). Capacitance reduction using ripple suppression control of single phase energy stored quasi-z-source inverter. In *11th International Scientific and Practical Conference Environment. Technology. Resources*, 15–17 June 2017 (pp. 154–158). Rezekne Academy of Technology.

12. Makovenko, E., Husev, O., Zakis, J., Roncero-Clemente, C., Romero-Cadaval, E., & Vinnikov, D. (2017). Passive power decoupling approach for three-level single-phase impedance source inverter based on resonant and PID controllers. In *11th IEEE International Conference on Compatibility, Power Electronics and Power Engineering*, 4-6 April 2017 (pp. 516–521). IEEE.
13. Lidow, A., Strydom, J., de Rooij, M., & Reusch, D. (2014). *GaN transistors for efficient power conversion*. New Jersey: Wiley.
14. Rothmund, D., Bortis, D., & Kolar, J. W. (2016). Accurate transient calorimetric measurement of soft-switching losses of 10kV SiC MOSFETs. In *IEEE 7th International Symposium on Power Electronics for Distributed Generation Systems (PEDG)*, 27–30 June 2016 (pp. 1–10). IEEE.
15. Hoffmann, L., Gautier, C., Lefebvre, S., & Costa, F. (2013). Thermal measurement of losses of GaN power transistors for optimization of their drive. In *15th European Conference on Power Electronics and Applications (EPE)*, 2–6 September 2013 (pp. 1–8). Lille, France.
16. Han, D., & Sarlioglu, B. (2016). Deadtime effect on GaN-based synchronous boost converter and analytical model for optimal deadtime selection. *IEEE Transactions on Power Electronics*, 31(1), 601–612.
17. Si826x: 5 kV LED Emulator Input, 4.0 A Isolated Gate Drivers . [Online]. Available at <https://www.silabs.com/documents/public/data-sheets/Si826x.pdf> [Accessed: 08-Aug-2017].
18. Zhao, C., Trento, B., Jiang, L., Jones, E. A., Liu, B., Zhang, Z., ... Langley, R. (2016). Design and implementation of a GaN-based, 100-kHz, 102-W/in³ single-phase inverter. *IEEE Journal of Emerging and Selected Topics in Power Electronics*, 4(3), 824–840.

GAN TRANSISTORU PIELIETOŠANAS APSVĒRUMI MIKROINVERTORĀ ENERĢIJAS UZKRĀJĒJU INTEGRĒŠANAI MAIŅSTRĀVAS TĪKLĀ

K. Kroičs, J. Zakis, A. Suzdaļenko, O. Husevs

Kopsavilkums

Šajā rakstā apskatīti izaicinājumi, kas jāņem vērā tradicionālajos Si tranzistoros, aizvietojo ar GaN tranzistoriem un paaugstinot invertora darba frekvenci. Paaugstinot darba frekvenci, liela uzmanība ir jāpievērš spiestās plates dizainam, pēc iespējas samazinot parazītiskās induktivitātes un kapacitātes. Tranzistoru ieslēgšanās un izslēgšanās straujumu var mainīt izvēloties attiecīgu aizvara pretestību: pārāk liela pretestība izsauc palielinātus komutācijas zudumus, bet pārāk maza pretestība izsauc zudumus aizvara kapacitātes pārlādē, ka arī strauju sprieguma izmaiņu, kas izsauc paaugstinātus elektromagnētiskos traucējumus, kā arī pārspriegumus. Tranzistora draivera barošanai var tikt izmantots bipolārs vai unipolārs spriegums. Negatīva sprieguma izmantošana ļauj pasargāties pret tranzistora kļūdainu atvēršanos, taču tranzistora zudumi, strāvai plūstot pretējā virzienā, pieaug. Strāva plūst pretējā virzienā laikā, kurā augšējā un apakšējā pleca tranzistori ir neaktīvā stāvoklī. Šāda stāvokļa ieviešana ir nepieciešama, lai novērstu īslaicīgu īslēgumu, kas rastos tāpēc,

ka tranzistora aizvēršanās process nav momentāns. Šo neaktīvā stāvokļa laiku, galvenokārt, nosaka draivera mikroshēmas aiztures laiku izkliede, tāpēc efektivitātes uzlabošanai paralēli var tikt pieslēgta ātrdarbīga diode ar mazāku sprieguma kritumu nekā GaN tranzistoram. Strāvu un spriegumu mērīšana var ietekmēt pārveidotāja darba režīmu, tāpēc ir jāizvēlas atbilstošas mērīšanas metodes. Rakstā ir parādīts uz GaN tranzistoriem balstīta invertora prototips un dotas dažas invertora oscilogrammas.

07.09.2017.

DOI: 10.1515/lpts-2017-0031

DYNAMIC AIR GAP CHANGE OF LOW-SPEED GENERATOR
CONSIDERING THERMAL EXPANSION, CENTRIFUGAL FORCE AND
MAGNETIC FORCE EFFECTS

M. Cerpinska, R. Elmanis-Helmanis
Riga Technical University,
1 Kalku Str., Riga LV-1658, LATVIA
e-mail: marina.cerpinska@rtu.lv

The paper provides the data collected over a three-year period to illustrate the dynamic air gap change depending on generation modes of four hydropower generators with similar design. The tests were performed on hydropower units at the rated apparent power of 105 MVA and the air gap of 20 mm. The results obtained showed that the average air gap change in different modes could reach up to 2.1 mm. Around 90 % of air gap change results from thermal expansion and 10 % were determined by centrifugal and magnetic forces. In coasting mode when the power was switched off and the speed of the generator decreased, the air gap increased up to 0.7 mm. Attraction forces resulting from magnetic phenomena accounted for 0.1–0.6 mm decrease in the air gap.

Keywords: *air gap, centrifugal force, hydropower unit, magnetic force.*

1. INTRODUCTION

Knowing the exact value of operational air gap is important for two reasons. Firstly, applying the correct values of the air gap ensures correct modelling and simulation results for the transient parameters of electrical machines [1]. Secondly, it provides valuable information for reliability check of the equipment.

When the condition monitoring of the hydropower generator is performed, the air gap is measured and evaluated. The evaluation requires comparing the actual air gap to its nominal value or the average value. According to the Institute of Electrical and Electronics Engineers (IEEE) manual p. 8.5.1 [2], air gap variation of ± 10 % from average is acceptable. It means that for the average air gap value of 20 mm, the distance between the rotor pole and stator could be either 18 mm or 22 mm. The static air gap of hydropower generator measured during the commissioning stage can be close to those required values, but the dynamic air gap measured during operation tends to vary more in different operational modes.

During the early measurements series in 2015, the minimum air gap measured on unit No. 1 in mode “Full speed no load (FSNL) excited 13.8 kV” was 18.1 mm, while the maximum air gap in mode “Coasting with 31 % rotational speed of rated

speed” was 20.2 mm (see Fig. 4 for more details). The difference between average values in those modes was 2.1 mm, but the difference between the minimum and maximum value reached 3.64 mm. While the variation of the rotor roundness and static air gap due to imperfection of fabrication and balancing was intuitive, the idea of the rigid rotor assembly contracting or expanding during operation seemed unrealistic and provided motivation for further investigation.

Researchers agree that the dynamic air gap or the operating air gap is different from the static air gap because the rotating assemblies are subject to centrifugal and magnetic forces [3]–[4]. The thorough description of stresses of rotating discs was addressed in the Journal of Applied Mathematical Modelling [5], but the change of the air gap could not be explained by rotor stresses only. Since the air gap is a distance measurement between the rotor pole and stator bar, it is affected both by rotor and stator movement. Stator does not rotate, but it is subject to thermal expansion effects, and as noted three decades earlier, it is more deformable than rotor and yields to a variety of forces [4]. According to Chapter 2.6 [6], the forces in the stator frame and foundation are massive, especially during instantaneous changes in generation modes. Therefore, the objective of the paper was to study simultaneously the temperature effects and the impact of centrifugal and magnetic forces on the air gap.

The site measurements showed that the air gap either decreased when the load was applied to the generator (see results in Section 4.3) or increased when the speed of the generator decreased (see results in Section 4.2), but the main variation was determined by thermal expansion. Indeed, the manufacturers today specify the nominal or designed air gap value both for “cold” and “hot” generator in the technical documentation and the difference between the two could be from 1.5 to 2 mm (for the units under study the rated “hot” air gap was 20 mm, and “cold” air gap was 18 mm).

The experimental results of the paper discuss the underlying factors for dynamic air gap change and provide some data collected over a three-year period to illustrate the specific air gap values depending on generation modes of four low-speed salient pole synchronous generators of the same design. In addition, a comparison of the air gap change and vibration results is provided.

2. THEORY

Centrifugal Force

The example of centrifugal force acting on a generator rotor is shown in Fig. 1. The model given in the handbook [7], which is adapted for particular design of units (size of assembly parts and bearing location), is discussed in the study.

The centrifugal force is not a concern of the small perfectly balanced rotating articles, but large generators (the units under study had rotor diameter of 11.62 m) on site could not realistically have zero unbalance, and therefore there is centrifugal force, while the unit rotates. The guidelines [8] provide an example for the ultimate situation when “at a runaway speed after a load rejection stresses can be three to four times higher than in rated operation”.

The centrifugal force is proportional to the speed of the unit as suggested by dynamic equation (1) [9]:

$$F_c = mr\omega^2, \quad (1)$$

where F_c – centrifugal force, N ; m – eccentrically located mass centre of the rotor, kg ; r – radius from eccentrically located mass to the rotation axis, m ; ω – angular speed of rotation, rad/s .

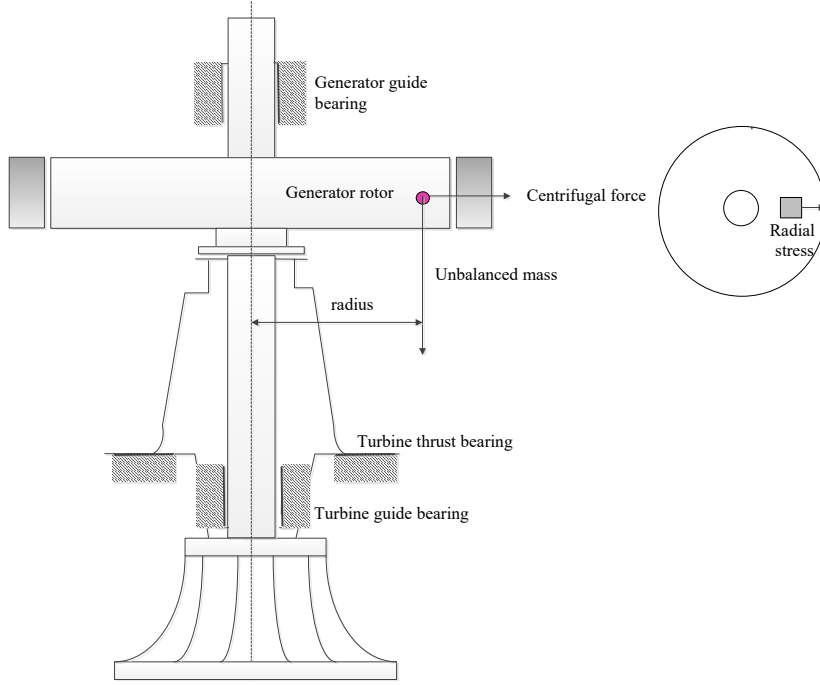


Fig. 1. Design of the unit and bearing location. Centrifugal force vector acting on hydropower generator, causing rotor to expand radially.

Following equation (1), as the speed decreases, the centrifugal force decreases. The stresses developed due to rotation and centrifugal forces in circular disks are circumferential stresses σ_c and radial stresses σ_r [10]–[11]. Considering the direction of these stresses, the size of the air gap is affected by the radial stress. Radial stress for a rotating solid disk at any radius r is calculated according to equation (2) [11]:

$$\sigma_r = \frac{\rho \cdot \omega^2}{8} (3 + \mu) [r_2^2 - r^2], \quad (2)$$

where σ_r – radial stress, N/m^2 ; ρ – density of material, kg/m^3 ; ω – angular speed of rotation, rad/s ; μ – Poisson's ratio; r – radius at any point of the disc, m .

Equation (2) shows that at a lower speed the radial stress developed due to the centrifugal force decreases because other variables do not change, since the radius is calculated from boundary conditions when stresses are zero [10]. Thus, the radial stress σ_r developed in the rotating disc depends only on angular speed ω squared.

To describe centrifugal force effects, coasting mode (natural deceleration of a generator when the power is removed) was studied. In coasting mode, excitation is switched off and magnetic forces can be considered negligible, and mainly the centrifugal force is acting on the generator rotor. Modes at different rotational speeds were analysed, starting from the rated rotational speed until the crawling speed equal to ~30 % of rated operational speed was achieved.

Magnetic Force

If there is a change in vibration when the load is applied, it means that there are unbalanced electrical exciting forces acting on the generator. Equation (3) for magnetic force is given as [7]:

$$F_m = \frac{S}{2\mu_0} B^2, \quad (3)$$

where F_m – magnetic force, N ; S – section area of the rotor pole, m^2 ; $\mu_0 = 4\pi \cdot 10^{-7}$, magnetic constant, also known as Vacuum Permeability, H/m ; B – magnetic field, T .

Magnetic force was evaluated by comparing “FSNL excited/ non-excited” modes. In “FSNL non-excited” mode there are no magnetic forces acting on the generator, while in “FSNL excited” mode there is no current flow in stator windings, but magnetic current is produced by the excitation windings [12].

Hydraulic Forces

Synchronous condenser or “condense” mode is compared with “FSNL non-excited” mode to study the effect of hydraulic forces because in synchronous condenser mode there is no water flow affecting the turbine [7]. For the present study, synchronous condenser mode with 0 MVar reactive power supplied back to the electrical grid was used.

3. EXPERIMENTAL PART

The tests were performed on four 105 MVA, 13.8 kV, 50 Hz hydropower units with umbrella-type hydrogenerators. Generator rotors had 68 salient rotor poles, rotor spider with 12 segments, rotation direction – clockwise. Stator had 14.62 m diameter and six segments with 504 stator slots. The rated speed of the units was 88.2 RPM. Nominal air gap was 20 mm. The design of the unit and bearing location is shown in Fig. 1. The design of the generator rotor is demonstrated in Fig. 2.

The “Meggit Vibro-Meter air-gap” measurement system ILS730 with sensor LS120 (sensitivity 0.3V/mm ($\pm 5\%$), range 0–33 mm) was used. The value of the air gap is measured in Volts and converted to millimetres according to manufacturer’s scale. In the earliest experiments of 2014–2016, two air gap sensors were used, placed at the top and at the bottom of the stator; in 2017 four sensors were

used, placed at the top of the rotor as shown in Fig. 2. Thus, two air gap sensors were used for generators No. 1 and No. 2. Four sensors were used for generators No. 3 and No. 4. Using more sensors allows for better analysis of the dynamic behaviour in case of unbalance. Table 1 summarises the history and location of the sensors for the present study.

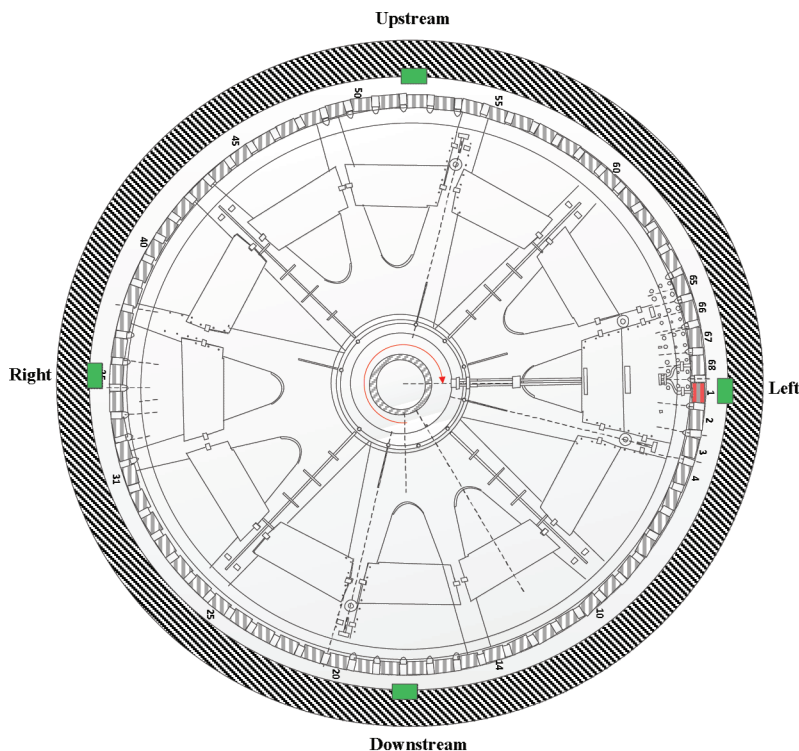


Fig.2. The top view of generator rotor and four air gap sensors (indicated green) are glued at the top of the stator. The first rotor pole is indicated red.

Table 1

Sensor Positions for Experiments

No.	Year	Unit	Measurement position
1	2014	No. 1	1 sensor on top
2	2015	No. 1	2 sensors (top and bottom, see Fig. 1 in [13])
3	2015	No. 1	2 sensors on top
4	2016	No. 2	2 sensors (top and bottom)
5	2016	No. 2	
6	2017	No. 3	4 sensors on top
7	2017	No. 4	

The units are presented in consecutive order in the paper according to measurement dates to meet the confidentiality policy of the owned power plant. The results in the following section are provided in the same sequence.

Invasive sensors glued on the stator provide good precision, but the stator roundness should be considered when absolute values of the air gap in millimetres

are conferred because stators in practice are rarely thoroughly even. Stator roundness was checked by attaching an invasive air gap sensor to one of the rotor poles, placing the measurement equipment inside the rotor for data recording and rotating the generator at a crawling speed. As a result, variation of measurement results from four sensors could be logically explained. The example of unit No. 3 is provided in Fig. 3, where downstream sensor air gap values were always greater than upstream values.

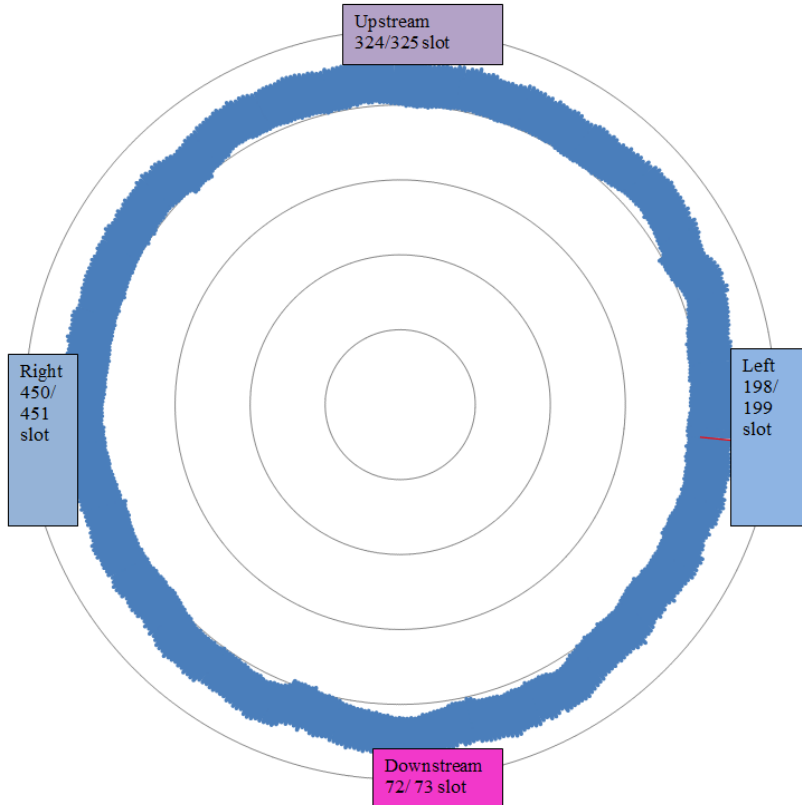


Fig.3. Stator shape, example for Unit No. 3, explaining different results of the air gap obtained from different sensors. The downstream sensor readings give the greatest value. Left and right sensor readings are the same.

4. RESULTS

The example of change of the average air gap in different generation modes is shown in Fig. 4, where the change depending on temperature is also demonstrated. Stator core temperature was obtained from the built-in condition monitoring system.

4.1. Temperature Change Effects on the Air Gap

Observations on site and expertise of other researchers investigating air gap size [14] suggested that the air gap changed significantly as the stator temperature

changed; therefore, the variation of the air gap during the generator warm-up and different modes was registered. The results are shown below in Fig. 4 for unit No. 1.

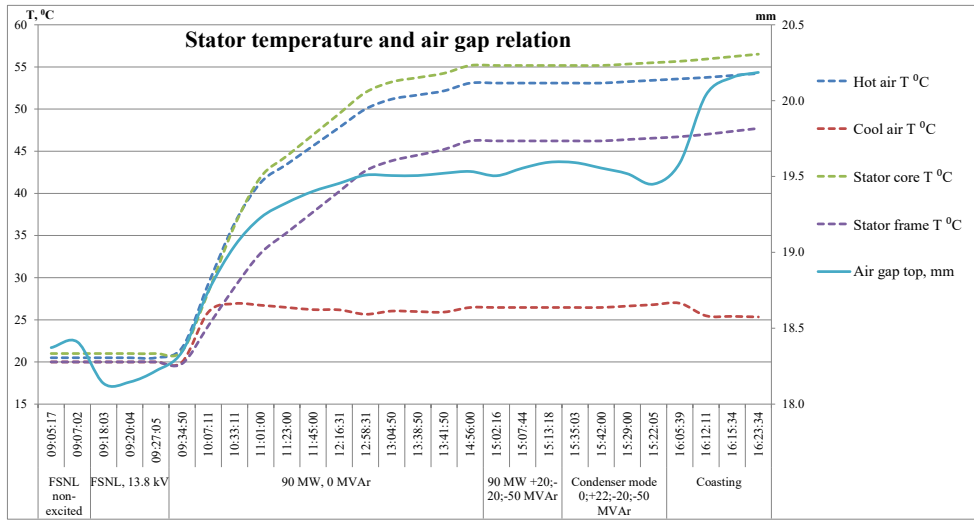


Fig.4. Air gap change in different operating modes.

The air gap change from temperature is best observed in mode “90 MW, 0 MVar”, when no other changes were applied to the unit. Correlation of air gap change and temperature change and stator wall movement due to thermal expansion was calculated, based on the sample correlation coefficient and the coefficient of determination [15]. Results are summarised in Table 2.

Table 2

Correlation of Air Gap Change from Temperature Change and Stator Wall Thermal Expansion for Unit No. 1

Correlation of air gap with:	Hot air T, °C	Cool air T, °C	Stator core T, °C	Stator frame T, °C	Displacement of the stator wall (relative to stator core)
Sample correlation coefficient, r	1.0	0.8	1.0	0.9	0.9
Positively correlated, $r > 0$?	yes				
Coefficient of determination	91 %	69 %	91 %	90 %	83 %
Correlation strength	strong	weak	strong	strong	strong

Although correlation measures association rather than causation, Table 1 together with Fig. 4 provides good evidence that 83 % of air gap growth can be explained by stator expansive displacement during warm-up, 7 % of air gap growth is caused by other thermal expansion phenomena or other underlying factors, and the remaining 10 % is determined by forces independent of temperature, such as centrifugal and magnetic forces.

4.2. Centrifugal Force Effect on the Air Gap

Figure 3 suggests that especially in coasting mode the change of the air gap could not be explained by the temperature change because temperature remains the same, while the air gap value grows. As suggested in the theory section, the centrifugal forces are the main factors acting on the generator during the coasting mode. It means that in this specific mode the correlation between angular velocity and the air gap should be strong. The results of the air gap of units No. 1, No. 2 and No. 3 in coasting mode provided in Table 3 justify this statement.

Table 3

Correlation of Air Gap at Speed in Coasting Mode of Units No. 1, No. 2 and No. 3

Unit No. 1	Speed, % of rated operation	Speed, RPM	Average air gap, top sensor	Average air gap, bottom sensor
	100 %	88.2	19.00	20.09
	64 %	56.6	19.44	20.56
	48 %	42.7	19.56	20.68
	40 %	35.6	19.59	20.72
	Sample correlation coefficient, r		-0.99	-0.99
	Positively correlated, $r > 0$?		No, negatively correlated	
	Coefficient of determination		98 %	98 %
	Correlation strength		strong	strong
Unit No. 2	Speed, % of rated operation	Speed, RPM	Average air gap, top sensor	Average air gap, bottom sensor
	100 %	88.0	23.12	24.50
	87 %	77.0	23.47	24.85
	63 %	56.0	23.69	25.10
	52 %	45.5	23.76	25.17
	49 %	43.0	23.77	25.18
	Sample correlation coefficient, r		-0.96	-0.96
	Positively correlated, $r > 0$?		No, negatively correlated	
	Coefficient of determination		92 %	93 %
	Correlation strength		strong	strong
Unit No. 3	Speed, % of rated operation	Speed, RPM	Average air gap of top upstream sensor, mm	
	60 %	52.9	21.67	
	50 %	44.1	21.76	
	44 %	38.8	21.79	
	39 %	34.4	21.81	
	35 %	30.9	21.82	
	Sample correlation coefficient, r		-0.97	
	Positively correlated, $r > 0$?		No, negatively correlated	
	Coefficient of determination		94 %	
	Correlation strength		strong	

The negative correlation in Table 3 indicates that for this data set a speed which is less than the rated speed is strongly associated higher than the designed value of the air gap. This is explained by equation (1) since the centrifugal force is smaller, when the rotation speed is lower.

Some values obtained for unit No. 2 appeared to be unreasonably large. Since the measured value of the air gap depends on earthing quality of the capacitive air gap sensor, the real values of air gap of unit No. 2 could be less. Nevertheless, the tendency of air gap change due to a decrease in the rotational speed is still conclusive.

4.3. Magnetic Pull Effect on the Air Gap

The difference between modes “FSNL non-excited” and “FSNL excited 13.8 kV” is distinct in Fig. 3. As soon as the load is applied to the generator, the air gap decreases. This is due to the fact that a magnetic phenomenon present in “FSNL excited 13.8 kV” mode produces forces of attraction, which act on the rotor and the stator. The specific decrease is shown in Table 4 (please see measurement positions and measurement years in Table 1).

Table 4

Results of Change in Air Gap in Modes Switching from “FSNL non-excited” to “FSNL excited 13.8 kV”

No.	Difference, average in mm	Comments on vibration
1	-0.3	Vibration was approximately the same.
2	-0.3	
3	-0.3 and -0.6	
4	-0.5	
5	-1.1 and -1	Vibration significantly increased on turbine thrust bearing. Temperature effects disrupted this experiment because when the mode of FSNL 13.8 kV was measured, the generator was still “cold”.
6	-0.1, -0.2, -0.3	Vibration increased both on generator guide bearing and turbine thrust bearing.
7	-0.1 and -0.2	Vibration was greater on turbine thrust bearing in “non-excited” mode.

4.4. Hydraulic Forces

To evaluate hydraulic effects, “Synchronous condenser” and “FSNL excited 13.8 kV” modes were chosen so that magnetic pull was similar in both modes, and additional unbalance was caused by hydraulic forces in “FSNL excited 13.8 kV” mode only. Results are shown in Table 5.

Table 5

**Results of Change in Air Gap and Vibration in Modes
“Synchronous Condenser” and “FSNL Excited 13.8 kV”**

No.	Air gap	Vibration
1	No distinctive difference	Greater in FSNL excited mode
2	Smaller in FSNL excited mode by 0.3 mm	Greater in FSNL excited mode
3	Greater in FSNL excited mode by 0.2 mm	No distinctive difference
4	Smaller in FSNL by 0.5 mm	Greater in FSNL excited mode
5	Generator was “cold” in one mode, data could not be used for comparison	Significantly greater in FSNL excited mode
6	No distinctive difference	Greater in FSNL excited mode
7	No distinctive difference	Significantly greater in FSNL excited mode

Vibration data in Table 5 illustrate that in condenser mode there is no water on the turbine, so the vibration values are smaller. Results 6 and 7 are the most informative because for those generators vibration was much higher in FSNL excited mode than in synchronous condenser mode, while air gap remained the same.

5. DISCUSSION

If the air gap were the same in all operation modes, it would have meant that the stator and rotor expanded uniformly. In the example of unit No. 1 in Fig. 3, the stator expanded faster than the rotor.

Some displacement data, omitted in the results section, showed that during the coasting mode the stator contracted a little bit due to the drop of cooling air flow temperature. On the contrary, the hot air did not change and the air gap increased as the generator speed decreased – Table 2 showed the strong negative correlation of speed and air gap size. The low speed was strongly associated with higher than designed value of the air gap. Equation (1) showed that the higher the speed, the higher the centrifugal force. Applying this principle to the coasting mode, at a speed of 43 RPM, the centrifugal force would be 24 % of the centrifugal force for the generator at the rated rotational speed of 88.2 RPM, and at the crawling speed of 34 RPM, the centrifugal force would be only 15 % compared to the rated speed. However, when less tensile outward forces act on the rotor poles, the rotor of hydropower generator could contract up to 0.7 mm during the crawling speed compared to its size in the rated operation.

Although the attraction forces resulting from magnetic phenomena are considered to be large [4], [16], the difference of the air gap after the load applied to the generator was not more than 0.6 mm. This is a little bit less than 1 mm (the value suggested by early developers of air gap measurement systems [4]).

6. CONCLUSIONS

1. The air gap growth during operation proved to be determined by stator expansive displacement during warm-up in the first place. The thermal expansion effects caused 90 % of the air gap variation.
2. In coasting mode the air gap growth proved to be determined by the decrease in speed of the generator and decrease of centrifugal force and resulting radial stress. The increase of the air gap up to 0.7 mm was registered at the crawling speed compared to the rated speed of rotation.
3. Magnetic phenomena accounted for 0.1–0.6 mm air gap change for the generators with nominal air gap of 20 mm. When magnetic forces were applied, the air gap became smaller due to attraction forces.
4. Hydraulic forces had no effect on the air gap during the present study. The change of turbine bearing vibration remained the best indicator of hydraulic force effects.

REFERENCES

1. Kokoko, O., Merkhoul, A., Tounzi, A., Al-Haddad, K., & Guillot, E. (2015). Analysis of air-gap influence on a large hydro generator's parameters using sudden symmetrical short-circuit test. In 2015 IEEE International Electric Machines & Drives Conference (IEMDC), 10–13 May 2015 (pp. 102–107). Coeur d'Alene, USA: IEEE. DOI: 10.1109/IEMDC.2015.7409044
2. IEEE Std 492™-1999 (R2011). IEEE Guide for Operation and Maintenance of Hydro-Generators.
3. Adamowski, J. C., Souza, A. T., Perez, N., Lima, A. A., Oda, P. D., & Tiba, H. H. (2013). Ultrasonic dynamic air-gap monitoring system for large hydro-generators. In IEEE Joint UFFC, EFTF and PFM Symposium, 21–25 July 2013 (pp. 1311–1314). Prague, Czech Republic: IEEE. DOI: 10.1109/ULTSYM.2013.0335
4. Talas, P., & Toom, P. (1983). Dynamic measurement and analysis of air gap variations in large hydroelectric generators. *IEEE Transactions on Power Apparatus and Systems*, v. PAS-102(9), 3098–3106. DOI: 10.1109/MPER.1983.5519300
5. Allam, M. N. M., Badr, R. E., & Tantawy, R. (2008). Stresses of a rotating circular disk of variable thickness carrying a current and bearing a coaxial viscoelastic coating. *Applied Mathematical Modelling*, 32(9), 1643–1656. DOI: 10.1016/j.apm.2007.06.002
6. Klempner, G., & Kerszenbaum, I. (2004). *Operation and Maintenance of Large Turbo-Generators* (Vol. 14). Hoboken, New Jersey: John Wiley & Sons.
7. Shtern, E. P. (1985). *Handbook on operation and repair of hydraulic turbine equipment*. Moscow: Energoatomizdat (In Russian: Справочник по эксплуатации и ремонту гидротурбинного оборудования / под ред. Е. П. Штерна. М.: Энергоатомиздат).
8. VDI 3839 Part 6. (2007). *Instructions on Measuring and Interpreting the Vibration of Machines – Typical Vibration Patterns with Machine Sets in Hydraulic Power Stations*.
9. Vinogradov, O. (2000). *Fundamentals of kinematics and dynamics of machines and mechanisms*. Boca Raton, Florida: CRC press.
10. Jindal, U. C. (2010). *Machine design*. India: Pearson Education.

11. Bansal, R. K. (2009). *A textbook of strength of materials* (4th ed.). New Delhi: Laxmi Publications.
12. Dirba, J., Ketners, K., Levins, N., & Pugacevs, V. (2002). Electric Vehicles in Transport: Textbook. Riga: Jumava. (In Latvian: Dirba, J., Ketners, K., Levins, N., Pugačevs, V. (2002). *Transporta elektriskās mašīnas: mācību līdzeklis*. Rīga: Jumava).
13. Griscenko, M., & Elmanis-Helmanis, R. (2015). Eccentricity of slow-speed salient-pole generator: Analysis based on air gap spectrum. *Latvian Journal of Physics and Technical Sciences*, 52(1), 26–37. DOI: 10.1515/lpts-2015-0003
14. Aguiar, A. B. M., Merkhof, A., & Al-Haddad, K. (2012). Influence of the air gap length on the magnetic core loss in large hydro generator. In 20th International Conference on Electrical Machines (ICEM), 2–5 September 2012 (pp. 328–332). Marseille, France: IEEE. DOI: 10.1109/ICEIMach.2012.6349886
15. Ross, S. M. (2004). *Introduction to probability and statistics for engineers and scientists* (3rd ed.). USA: Elsevier Academic Press.
16. Dirani, H. C., Merkhof, A., Giroux, A. M., & Al-Haddad, K. (2014). Study of the impact of eccentricity in large synchronous generator with finite elements. In International Conference on Electrical Machines (ICEM), 2–5 September 2014 (pp. 277–282). Berlin, Germany: IEEE. DOI: 10.1109/ICELMACH.2014.6960193

HIDROAGREGĀTA ĢENERATORA DINAMISKĀS GAISA SPRAUGAS IZMAIŅAS TERMISKĀS IZPLEŠANĀS, CENTRBĒDZES UN MAGNĒTISKO SPĒKU IETEKMĒ

M. Čerpinska, R. Elmanis-Helmanis

K o p s a v i l k u m s

Darbā ir apkopoti rezultāti, kas iegūti četriem vienādas uzbūves hidroagregātu ģeneratoriem triju gadu laikā, pētot dinamiskās gaisa spraugas izmaiņas, atkarībā no darba režīmiem. Pārbaudes veiktas hidroagregātiem ar nominālo pilno 105 MVA jaudu un 20 mm gaisa spraugu. Iegūtie rezultāti liecina, ka gaisa sprauga dažādos darba režīmos var vidēji izmainīties par 2.1 mm. Aptuveni 90% no gaisa spraugas izmaiņas ir skaidrojamas ar termiskās izplešanās procesu, bet 10% ir skaidrojamas ar centrālās un magnētiskās spēku ietekmi. Izskrējiena režīmā, kad slodze tiek noņemta, un rotācijas ātrums pakāpeniski samazinās, gaisa spraugas palielinājums var būt līdz 0.7 mm. Magnētisko pievilkšanās spēku ietekmē gaisa spraugas samazinājums var būt no 0.1 līdz 0.6 mm.

04.07.2017.

DOI: 10.1515/lpts-2017-0032

THEORETICAL AND EXPERIMENTAL RESEARCH OF SYNCHRONOUS
RELUCTANCE MOTOR

R. Dobriyan, S. Vitolina, L. Lavrinovicha, J. Dirba

Riga Technical University,

12/1 Azenes Str., Riga, LV-1048, LATVIA

e-mail: janis.dirba@rtu.lv

The paper presents the research on evaluation of accuracy of magnetic field calculations of synchronous reluctance motor in comparison with the results obtained in experiments. Magnetic field calculations are performed with the finite element method to determine values of the magnetic flux and electromagnetic torque according to the current value in motor stator and load angle between the rotor direct-axis and axis of stator magnetomotive force (MMF). Experimental values of magnetic flux and electromagnetic torque are obtained on motor with locked rotor while equivalent direct current is applied to the stator windings. The research shows that the results obtained from the magnetic field calculations coincide well with the experimental data.

Keywords: *electromagnetic torque, magnetic field calculations, magnetic flux, synchronous reluctance motor*

1. INTRODUCTION

Nowadays it is obvious that the intensity of usage of electrical machines increases as well as specific electromagnetic loads. It sets higher requirements for accuracy of calculations for electrical machines, as well as for the study of magnetic field that can be achieved taking into account detailed geometry of the machine and magnetic circuit saturation. It is also important to determine whether the results of magnetic field numerical calculations comply with real experimental data.

Various methods can be applied for magnetic field calculation in electrical machines, but the simplest way for considering magnetic circuit saturation is to perform numerical calculations based on Maxwell equations [1]. Since the energy conversion process mainly takes place in the active part of the electrical machine, it allows performing magnetic field calculations in two-dimensional space, i.e., magnetic field induction B and intensity H vary in radial and tangential directions, while in axial direction of machine their values remain constant.

The most frequently used method for magnetic field calculation is the finite element method FEM [2]–[10]. The benefits of FEM compared to other methods are the following: the possibility to define the object of any form; the ability to change

the discretization for different areas in order to obtain higher accuracy of calculations with finer mesh, and the possibility to define the boundary conditions of any length limits.

Magnetic field calculation using the finite element method allows determining the main parameters of electrical machine – magnetic flux, electromagnetic torque, values of magnetic induction in different parts of magnetic circuit, armature reaction inductive reactance and other parameters.

In the paper magnetic field calculations are performed for the synchronous reluctance motor (SRM), and in order to determine their accuracy the obtained results are compared to the experimental data.

2. THEORETICAL RESEARCH OF SYNCHRONOUS RELUCTANCE MOTOR

Within the framework of the research, low-speed synchronous reluctance motor SRM presented in Fig. 1 is used as the experimental object. Such motors are used in control systems of nuclear power stations if the motor is connected to 1–1.5 Hz AC power supply [11]. Parameters of the experimental motor are listed below:

the stator outer diameter	$D = 110 \text{ mm};$
the stator package length	$l = 222 \text{ mm};$
the air gap value	$\delta = 1.3 \text{ mm};$
the Carter coefficient	$k_c = 1.2;$
the number of pole pairs	$p = 2;$
the number of phases	$m = 3;$
the number of windings in phase	$w = 200;$
the winding coefficient	$k_w = 0.935;$
the number of stator teeth	$Z = 24;$
the value of nominal current	$I_1 = 10.8 \text{ A}.$

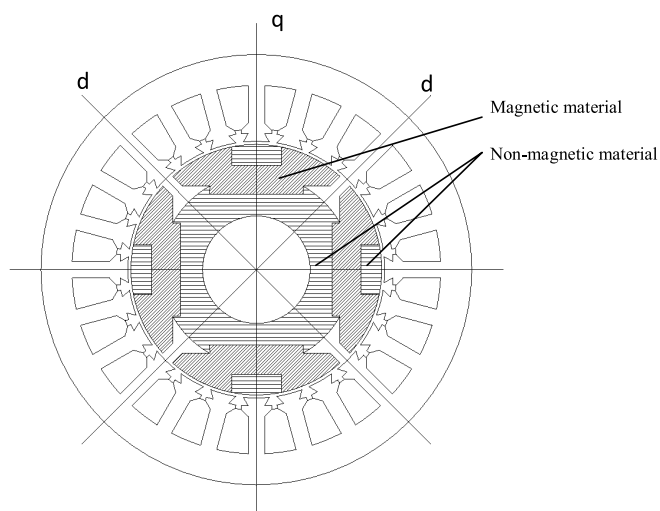


Fig.1. SRM construction.

All the required information about magnetic field of the electrical machine, including real saturation of magnetic circuit, can be obtained performing magneto-static field calculations based of Maxwell equations [2], [12].

Magnetostatic fields are produced by steady state currents, and magnetic field can be described using the following equations:

$$\text{rot} \vec{H} = \vec{j} ; \quad (1)$$

$$\text{div} \vec{B} = 0 ; \quad (2)$$

$$\vec{B} = \mu \mu_0 \vec{H} , \quad (3)$$

where H is the magnetic field intensity;

B is the magnetic field induction;

j is the current density;

μ is the magnetic permeability;

μ_0 is the permeability constant ($\mu_0=4\pi \cdot 10^{-7}$, H/m).

Magnetic flux of one pole of electrical machine can be defined as integral (4) in air gap for area S_1 which corresponds to one pole of electrical machine.

$$\Phi = \int_{S_1} B_1 dS_1 , \quad (4)$$

where B_1 is the magnetic induction in air gap;

S_1 is the surface corresponding to one pole.

The magnetic flux Φ curves for different values of current can be used to calculate voltage U_1 by using the amplitude values of the first harmonic of the magnetic flux Φ_1

$$U_1 = E_1 = 4.44 f w k_w \Phi_1 , \quad (5)$$

where E_1 is the phase EMF generated by the first harmonic of the magnetic flux;

f is the frequency of the current I_1 ;

w the number of windings in phase;

k_w is the winding coefficient.

Functions $\Phi=f(I_1)$ that are obtained for load angles $\Delta=0^\circ$ and $\Delta=90^\circ$ between the rotor direct-axis and axis of stator MMF represent magnetization curves respectively by direct-axis and quadrature-axis of the machine. Using these curves, it is possible to calculate direct-axis and quadrature-axis armature reaction inductive reactance x_{ad} and x_{aq} , respectively. Armature reaction inductive reactance x_{ad} and x_{aq} can be used in order to calculate electromagnetic torque value T_{em} using equation (6) [11], [13].

$$T_{em} = \frac{mI_1^2}{2\Omega}(x_{ad} - x_{aq})\sin(2\Delta) = \frac{mI_1^2}{2 \cdot 2\pi \cdot f_1}(x_{ad} - x_{aq})\sin(2\Delta), \quad (6)$$

where x_{ad} is direct-axis armature reaction inductive reactance;
 x_{aq} is quadrature-axis armature reaction inductive reactance;
 Ω is the angular rotation frequency.

Numerical calculation of two-dimensional magnetic field is based on a grid surface that is perpendicular to the shaft of the machine. The assumption is used that the length l of the machine is divided into n layers. Each layer has a thickness b_{sl} equal to l divided by n . Since the stator slots are skewed by a stator tooth pitch those layers are rotated by an angle α/n relative to one another, where α corresponds to a total angle of the slot skew (Fig. 2).

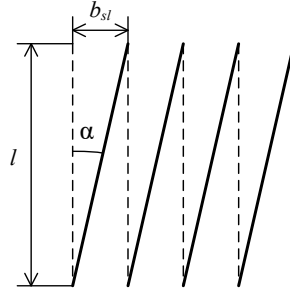


Fig.2. Graphical illustration of the skewed stator teeth (l – stator package length, α – total angle of the slot skew, b_{sl} – thickness of the skew corresponding to tooth pitch). Magnetic field calculations for the current task are performed by using calculations based on the finite element method. These calculations are performed through magnetostatic field simulations in *QuickField* software. This is a two-dimensional finite element analysis system from *Tera Analysis* [14].

In Fig. 3, the results of magnetic field calculations in *QuickField* software are represented as magnetic field lines corresponding to direct-axis when load angle $\Delta=0^\circ$ and to quadrature-axis when load angle $\Delta=90^\circ$.

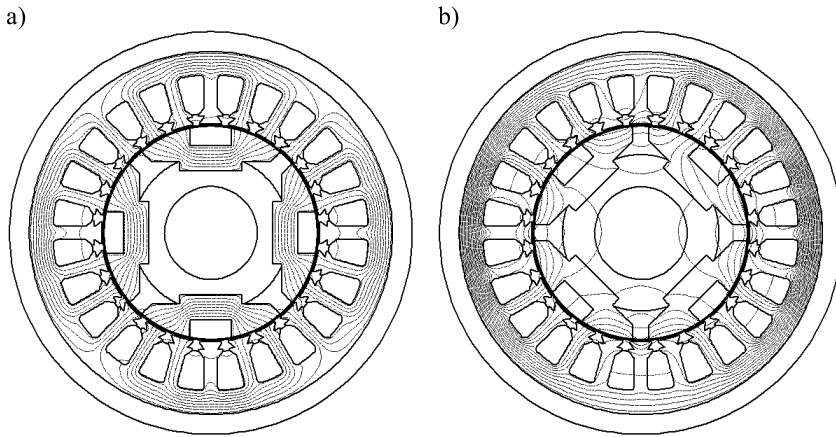


Fig.3. Depiction of magnetic field of SRM corresponding to (a) direct-axis and (b) quadrature-axis.

Figure 4 demonstrates magnetic flux curves for current values $I_1=4$ A and $I_1=12$ A, where load angle Δ varies within the range of 10° to 80° . These curves show both theoretically obtained values and experimental values measured with measuring windings 1–13. Experimental research of synchronous reluctance motor is described in Chapter 3 of the paper.

Curves given in Fig. 4 indicate that magnetic flux of the electrical machine depends not only on current value I_1 , but also on the operation mode, which is represented in form of angle Δ .

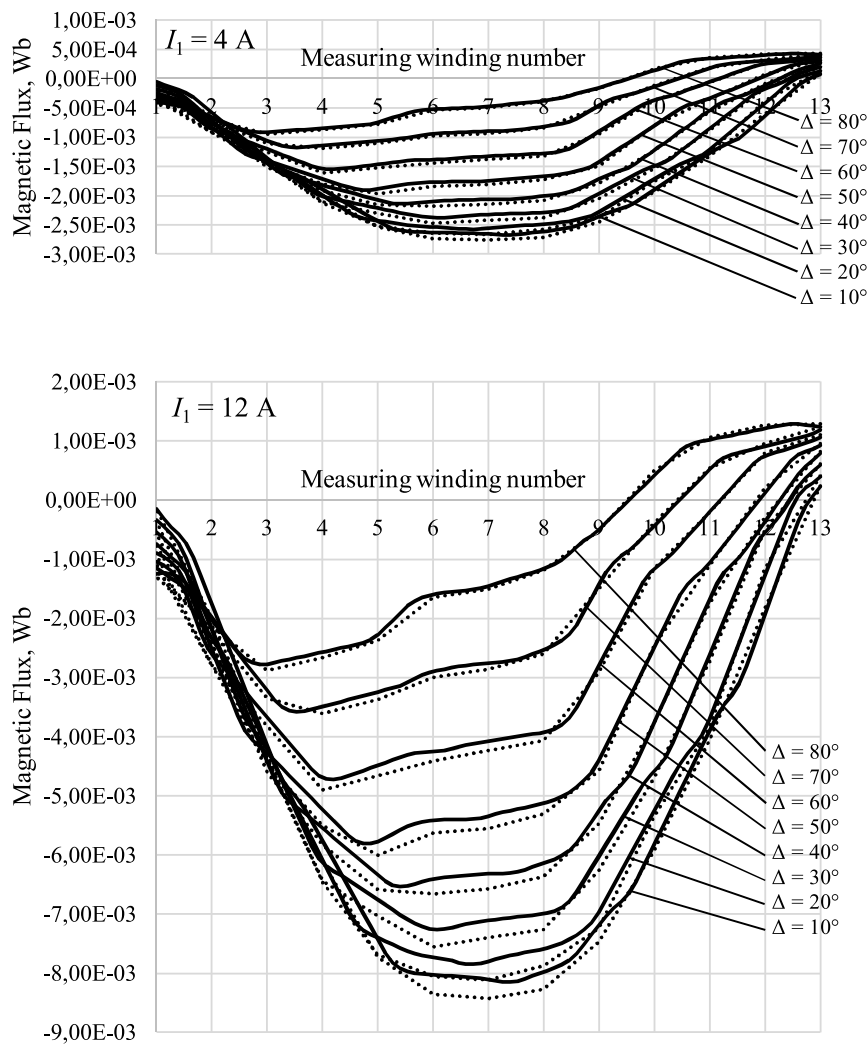


Fig.4. Values of magnetic flux for different values of current I_1 and load angle Δ
 — calculated values, experimental values.

Magnetic flux curves for different values of current I_1 , when load angle $\Delta=0^\circ$ and $\Delta=90^\circ$, are shown in Fig. 5 and can be used to calculate direct-axis and quadrature-axis armature reaction inductive reactance x_{ad} and x_{aq} , respectively.

Theoretical and experimental values of electromagnetic torque are presented in Fig. 6.

Values of electromagnetic torque are calculated using Maxwell stress tensor [15]. The electromagnetic torque is described with surface integral (7) over the closed surface S in the middle of the motor air gap.

$$T_{em} = \oint_S \left(\vec{r} \times \left[\frac{1}{2\mu_0} (B_n^2 - B_t^2) \times \vec{n} - \frac{1}{\mu_0} B_n B_t \vec{t} \right] \right) dS, \quad (7)$$

where T_{em} is the electromagnetic torque;

\vec{n} is the normal vector of the point on the closed surface S ;

\vec{r} is the radius-vector of the point on the closed surface S ;

\vec{t} is the tangent vector of the point on the closed surface S ;

B_n is the normal component of the magnetic flux density;

B_t is the tangential component of the magnetic flux density.

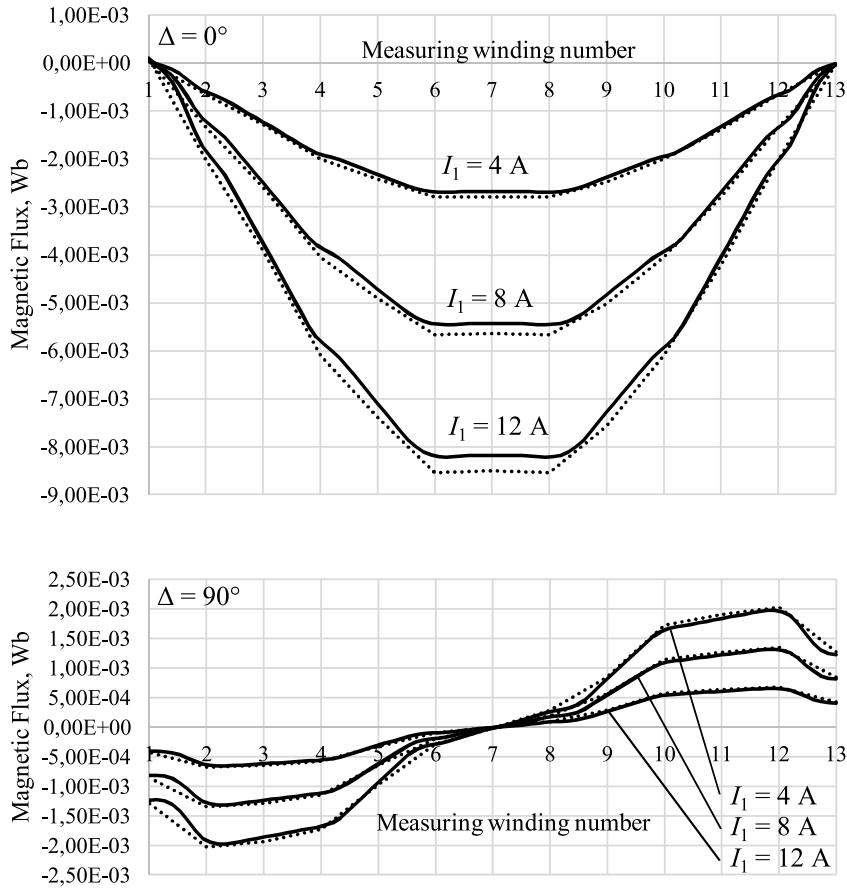


Fig. 5. Magnetic flux values for load angle $\Delta=0^\circ$ and $\Delta=90^\circ$
 — calculated values, experimental values.

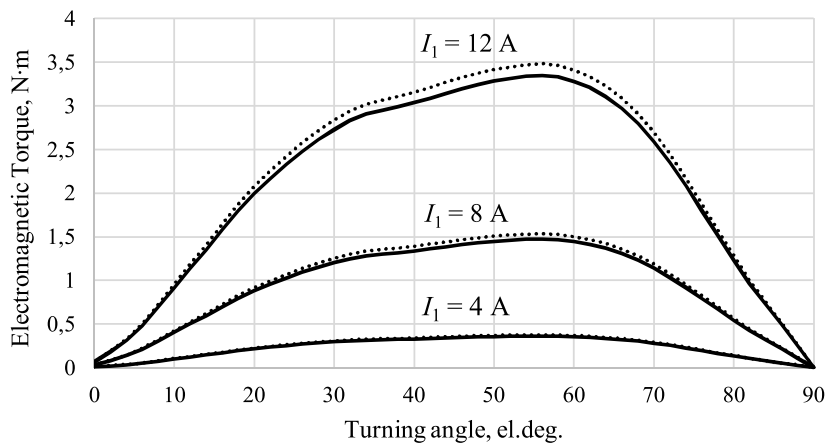


Fig. 6. Electromagnetic torque curves for different values of current I_1 for SRM with locked rotor calculated values, experimental values.

3. EXPERIMENTAL RESEARCH OF SYNCHRONOUS RELUCTANCE MOTOR

Theoretical calculation results obtained earlier can be confirmed by conducting experiment on the motor with locked rotor. Magnetic flux is measured with miliwebermeter. For the machine with rotating magnetic field magnetic flux Φ and voltage $U_1 = E_1$ are periodically variable parameters that can be determined by using measuring windings, placed on pole pitch τ where EMF E_1 is induced. In order to obtain the variation in time of magnetic flux Φ which is generated by the EMF, it is required to place n measuring windings on rotor as it is shown in Fig. 7.

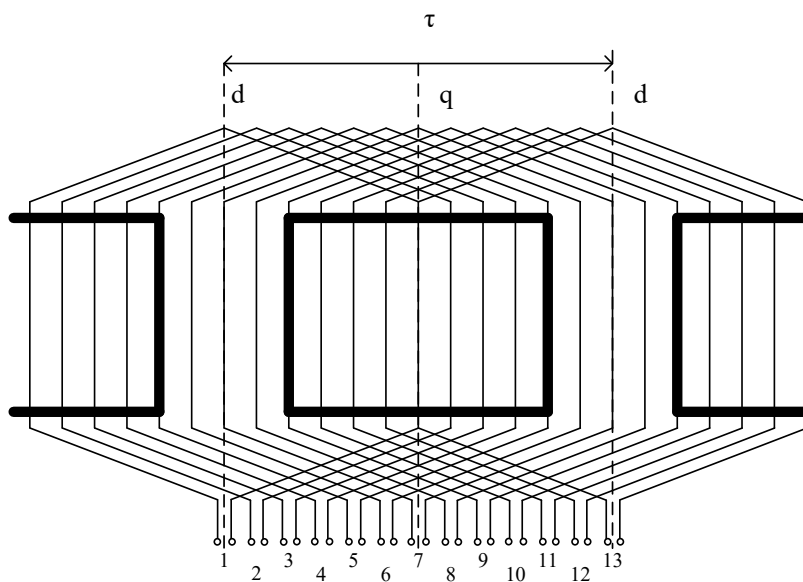


Fig. 7. Experimental SRM measuring winding placement scheme.

Equivalent direct current $I_{\text{e}} = \sqrt{2} \cdot I_1$ is applied to the stator phase windings of researched SRM with locked rotor. The first harmonic of magnetomotive force generated by the direct current I_{e} for the motor with locked rotor must be equal to the first harmonic of the magnetomotive force generated by the alternating current I_1 flowing in all 3 phases of the stator phase windings when the rotor rotates [13], [16].

By measuring magnetic flux Φ passing through areas 1–13 covered by measuring windings (Fig. 7) for different I_1 values, variable magnetic flux Φ for one half-period is obtained. Curves corresponding to magnetic flux Φ obtained by calculations and experiments are shown in Figs. 4 and 5.

Electromagnetic torque curves as function $T_{\text{em}} = f(I)$ can be experimentally obtained by using motor with locked rotor, when stator windings are supplied with DC current I_{e} . Direct current I_{e} flowing through the stator windings creates magnetic flux that interacts with permanent magnets and holds the rotor in the certain position. For the creation of static moment on the rotor the weight is applied to the rotor. Under the impact of the torque the rotor rotates at a certain angle that can be read from a disk with graduated scale. The value of rotor rotating angle depends on the weight suspended to the rotor.

Calculated and experimental electromagnetic torque curves are shown in Fig. 6. These curves show that theoretical and experimental results have decent compatibility.

4. CONCLUSIONS

Based on the results obtained within the framework of conducted research, the following conclusions can be drawn:

1. Magnetic flux curves and electromagnetic torque curves, as well as armature reaction inductive reactance and other parameters can be conveniently determined for synchronous reluctance motor with locked rotor.
2. Values of magnetic flux and electromagnetic torque obtained from numerical calculations of magnetic field with the finite element method coincide well with the experimental data. Results differ by 3 % to 7 % depending on the saturation level of magnetic circuit.
3. If magnetic circuit saturation is low, in order to determine load angle curves of synchronous reluctance motor it is possible to use values of armature reaction inductive reactance obtained from the magnetic field calculations with theoretical formulas of electrical machines.

ACKNOWLEDGEMENTS

The present research has been supported by the State Research Programme “LATENERGI” and developed within the framework of doctoral study grant of Riga Technical University.

REFERENCES

1. Maxwell, J.C. (author), & Niven, W.D. (editor) (2010). *The scientific papers of James Clerk Maxwell* (Volume I). New York: Cambridge University Press.
2. Claycomb, J.R. (2010). *Applied electromagnetics using QuickField and Matlab*. Jones and Barlett Publishers.
3. Bianchi, N., & Bolognani, S. (2000). Reducing torque ripple in PM synchronous motors by pole shifting. In *Proceedings of the International Conference on Electrical Machines, ICEM*, Aug. Helsinki.
4. Bianchi, N., Bolognani, S., Bon, D., & Dai Pré, M. (2009). Rotor flux-barrier design for torque ripple reduction in synchronous reluctance and PM-assisted synchronous reluctance motors. *IEEE Trans. Ind. Appl.*, 45(3), 921–928.
5. Moghaddam, R.R. (2011). *Synchronous reluctance machine in variable speed drives applications*. Doctoral Thesis. Stockholm, Sweden.
6. Reece, A.B.J., & Preston, T.W. (2000). *Finite elements methods in electrical power engineering*. Oxford: Oxford University Press.
7. Xiaohua, B., Na, L., Yong, F., & Fuying, L. (2015). Novel method of evaluation of Carter factor for closed slot submersible motor including fringing effect and magnetic saturation. *Transactions of China Electrotechnical Society*, 30(12), 220–227.
8. Oprea, C., Dziechciarz, A., & Maris, C. (2015). Comparative analysis of different synchronous reluctance motor topologies. In *Environment and Electrical Engineering (EEE-IC), 2015 IEEE 15th International Conference*. DOI: 10.1109/EEEIC.2015.7165464.
9. Sarac, V. (2010). Different approaches of numerical analysis of electromagnetic phenomena in shaded pole motor with application of finite elements method. In *XX URSI Commission B international symposium on electromagnetic theory*, Aug. 2010 (pp. 97–100), Berlin, Germany.
10. Lopez-Fernandez, X.M., & Gyselink, J. (2006). Finite element analysis of outer-rotor permanent magnet brushless DC motor for light traction. *COMPEL*, 25, 705–712.
11. Kanter, V.K. (1983). *Parameters and characteristics of salient-pole synchronous machines with a saturated magnetic core in steady-state symmetric modes*. Riga: Zinatne (in Latvian).
12. Zviedris, A. (2001). *Electrical machine electromagnetic calculations*. Riga: RTU Press. (in Latvian).
13. Lavrinovicha, L., & Dirba, J. (2015). *Brushless synchronous motors with external rotor*. Riga: RTU Press. (in Latvian).
14. Tera Analysis. (2010). *QuickField. Finite Element Analysis System. Version 5.7*. Denmark: Tera Analysis. Available at <http://www.quickfield.com>.
15. Bianchi, N. (2005). *Electrical machine analysis using finite elements*. CRC Press, Boca Raton, FL, Taylor & Francis.
16. Lavrinovicha, L., Dirba, J., Brakanskis, U., & Lavrinovich, N. (2013). Experimental study of synchronous electronically commutated outer-rotor brushless motor at stalled rotor. *Power and Electrical Engineering*, 31, 112–116.

SINHROŅĀ REAKTĪVĀ DZINĒJA TEORĒTISKĀ UN EKSPERIMENTĀLĀ IZPĒTE

R. Dobrijans, S.Vītoļiņa, L. Lavrinoviča, J. Dirba

Kopsavilkums

Novērtēta sinhronā reaktīvā dzinēja magnētiskā lauka aprēķinu precizitāte, salīdzinot to rezultātus ar eksperimentāliem mērījumiem. Magnētiskā lauka aprēķini veikti ar galīgo elementu metodi, nosakot magnētiskās plūsmas un elektromagnētisko griezes momentu atkarībā no dzinēja statora strāvas lieluma un slodzes leņķa starp rotora garenasi un statora MS asi. Plūsmas un momenta eksperimentālie mērījumi veikti dzinējam ar nobremzētu rotoru, barojot tā statora tinumus ar ekvivalento līdzstrāvu. Parādīts, ka no magnētiskā lauka aprēķiniem iegūtie rezultāti labi sakrīt ar eksperimentu datiem.

02.05.2017.

DOI: 10.1515/lpts-2017-0033

DEVELOPMENT AND ASSESSMENT OF PLANETARY
GEAR UNIT FOR EXPERIMENTAL PROTOTYPE OF
VERTICAL AXIS WIND TURBINE

A. Urbahs, M. Urbaha, K. Carjova

Institute of Aeronautics, Riga Technical University,

1 Kalku Str., Riga, LV-1658, LATVIA

aerti@rtu.lv

The theoretical calculation for development of planetary gear unit of wind turbine (WT) and its experimental tests are presented in the paper. Development of experimental prototypes from composite materials is essential to determine capability of element and its impact on feature. Two experimental scale prototypes of planetary gear unit for WT were developed for such purposes. Hall transducer, servomechanisms and optical tachometers were used to obtain results, comparison analysis of theoretical and actual data was performed as well as quality assessment of experimental prototypes of planetary gear unit. After kinematic and load analysis as well as control of rotation frequency, it is possible to declare that the unit is able to operate at designated quality. Theoretical calculations and test results obtained are used for industrial WT prototype development.

Keywords: *planetary gear, reduction gear, vertical rotation axis, wind turbine*

1. INTRODUCTION

Wind turbines (WTs) can be classified either by the aim of application or by their effectiveness, which is indicated by the conceptual scheme of wind turbine – type of rotation axis and rotor. WT can have both horizontal and vertical rotation axes. Turbines with horizontal rotation axis are called collinear, while turbines with vertical rotation axis [3]–[5], [7], [8], [10] – orthogonal. Turbine with horizontal rotation axis is called collinear because its efficiency directly depends on the direction of the wind. According to Albert Betz's law, maximum possible power coefficient that might be obtained in real environment by WT is $\xi = 0.593$ [1]. Nowadays, collinear WT may reach power coefficient in the range of $\xi = 0.46 \div 0.47$ [2], [7]. It means that the efficiency of these WTs are up to 47 % of air flow energy and it is notably close to a maximum possible value.

However, the analysis of practical use of WTs shows several significant disadvantages [6]:

- big financial contribution to the power unit obtained in comparison with other types of power plants;
- high operational costs to the power unit obtained;
- infra-sound made by wind turbines and impact on the environment;
- high risk of damage in case of sudden increase of wind speed.

Lack of efficiency can be solved with use of planetary gear unit in the structure of WT. Its compactness and high efficiency means that it is suitable for almost any metal working machine and can replace any type of industrial gear unit.

Load in the planetary gear unit is divided into several flows depending on a number of satellite gears, and satellite gears are already located symmetrically in the design state, allowing us to improve the following factors:

- dimensions of gears are reduced and manufacturing costs of reduction gear are reduced;
- noisiness of reduction gear is reduced;
- basic structure is simplified and energy losses are reduced;
- a number of grades are reduced by increasing transmission ratio and, thus, manufacturing costs of reduction gear are also reduced.

2. DETERMINATION OF TECHNICAL FEATURES OF WT PLANETARY GEAR UNIT

To determine technical features of planetary gear unit for WT, theoretical calculations and experimental tests were performed. Initial data of planetary gear unit are shown in Table 1.

Table 1

Initial Data of Planetary Gear Unit

Parameter	Value
Rated power, kW	100
Torque (at rated power), Nm	12000
Rotation speed (side of rotor), rpm	40
Rotation speed (side of generator), rpm	400–500

After kinematic calculations, ratios between the first and the second stages of reduction gear as well as the total ratio were obtained: $i_{H2-H1} = 3.5$, $i_{H1-1} = 2.9$ and $i_{sum} = i_{H2-H1} \cdot i_{H1-1} = 10.15$. Taking into account these ratios, rotation frequency at the rated rotation speed was determined (see Fig. 1).

In Fig. 1 green line reflects the ratio of the first stage control rotation speed (x axis) and the output rotation speed of the rotor (y axis). Blue line reflects the ratio of the input speed of the rotor (x axis) and the first stage central gear rotation speed (y axis). Red line reflects the ratio of second gear input speed of the rotor (x axis) and second gear output rotation speed of the rotor (y axis).

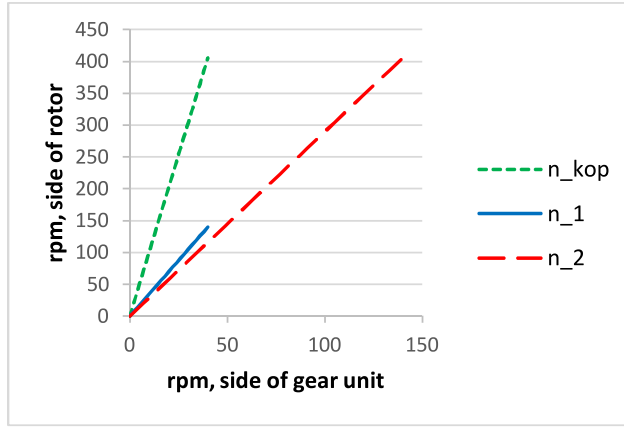


Fig.1. Rotation speeds – side of generator, rpm (y axis), side of rotor, rpm (x axis), side of planetary gear unit.

3. ANALYSIS OF WT POWER LOAD

It is mandatory to determine whether the chosen material has enough strength to withstand the calculated contact stress of gear teeth. For such purposes, steel 41CrMo was evaluated. Strength of material at allowable stress is calculated using the following formula (1) [9]:

$$\sigma_H \geq [\sigma_H], \quad (1)$$

where σ_H is maximum stress in the active surface of gear tooth (MPa) and $[\sigma_F]$ is material allowable contact stress (MPa).

Calculations showed that contact stress did not exceed maximum stress for any gear (see Fig. 2).

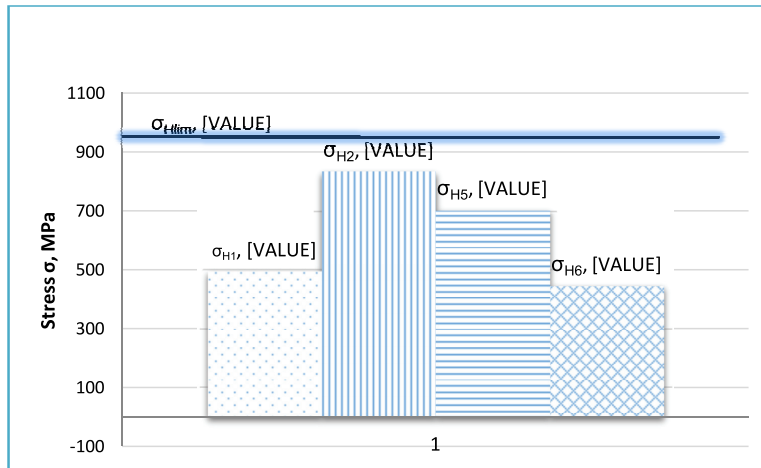


Fig.2. Maximum stress of planetary gear unit.

4. ROTATION FREQUENCY CONTROL OF WT PARTS

Rotation frequency control of WT parts is necessary to determine losses of energy and possible damage of a planetary gear unit [11]. Using results obtained theoretically, it is possible to test a planetary gear unit and obtain its operation parameters – rotation frequencies, input, and output rotations per minute (rpm) etc. for inner elements. Two experimental WT planetary gear unit prototypes at a scale of 1:10 and 1:5 were designed and manufactured for such purposes (see Fig. 3)

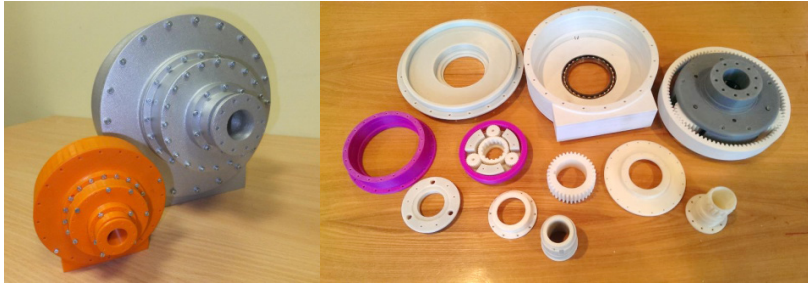


Fig.3. Experimental WT planetary gear unit prototypes and their elements.

Along with prototypes, test bench equipped with servomechanism “SM-S4315R 360 degree Servo Spring” was developed to obtain planetary gear unit rpm (see Table 2).

Table 2

Main Parameters of Servomechanism “SM-S4315R 360 Degree Servo Spring”

Parameter	Value
Rotation speed	0.16 s/60°
Voltage, V	6
Torque, kg/cm	15.4
Rotation time, s	0.96

Servomechanism allows adjusting supply voltage and input rpm. To estimate output rpm, either Hall transducer or optical tachometer is used. To ensure the accuracy of results, both methods were used (see Fig. 4).

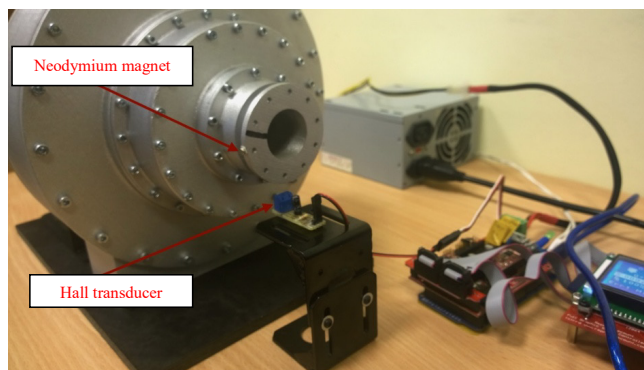


Fig.4. Output rpm control with Hall transducer.

During rotation speed tests, losses of friction were taken into account and maximum speed values (at the side of rotor 60–62 rpm, at the side of generator 530–580 rpm) were obtained. These results comply with the theoretically analysed results.

During industrial prototype tests at the scale of 1:1, rotation frequencies can be adjusted by Hall transducers that are connected in electric circuit. In case rotation speeds exceed maximum limits, control module will give a signal to brakes in order to reduce rotation frequencies.

5. KINETIC ANALYSIS OF WT PLANETARY GEAR UNIT

Kinetic analysis was performed in accordance with R. Willis methodology – the 2nd stage planetary gear unit was assumed to be fixed carrier H and the speed of the adjusted mechanism was determined (see Table 3).

Table 3

Rotation Indications

No.	Initial rotation indications	Adjusted rotation indications
1	$n_1 - n_A$	$n_1 - n_H$
3	$n_3 - n_B$	$n_1 - n_H$
H	n_H	$n_H - n_H = 0$

To determine transfer relation with fixed carrier H , the following formula (2) can be used [9]:

$$n_H = \frac{n_A \cdot z_1 + n_B \cdot z_3}{(z_1 + z_3)}. \quad (2)$$

Satellite gears S1; S1-2; S1-3; S2-1; S2-2; S2-3 of both prototypes were analysed at rotation speeds $Rl = 50..450$ rpm and $Rl = 500..900$ rpm (see Table 4).

Table 4

Results of Satellite Gears at $Rl = 500..900$ rpm

	A	B	C	D	E	F	G	T1	T2
Rl, rpm	500	550	600	650	700	750	800	850	900
M, mm	7	11	12	14	18	19	21	22	24
S1-1	14	15	17	21	23	24	25	27	29
S1-2	39	41	42	44	47	48	51	55	57
S1-3	25	27	29	28	28	32	33	34	37
S2-1	61	65	67	69	65	70	72	75	77
S2-2	59	62	62	61	64	67	69	70	72
S2-3	75	75	77	78	79	81	85	81	92

From these results it can be concluded that a planetary gear unit works in accordance with design parameters and theoretical calculations.

Linear speed and acceleration are depicted in graphs (see Figs. 5–6).

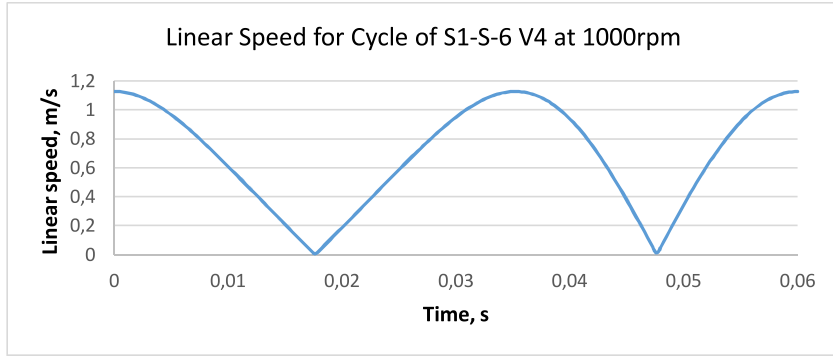


Fig.5. Time-dependent behaviour of linear speed, m/s.

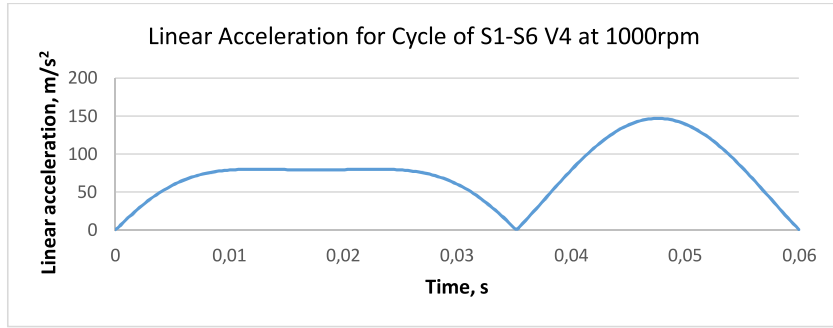


Fig.6. Time-dependent behaviour of linear acceleration, m/s².

Many factors that may affect safety, maintenance, environmental safety, costs etc. are taken into account during design and development of a planetary gear unit. To reach maximum efficiency, the following conditions should be met [9]:

- the number of teeth z_1, z_2, z_3, \dots is an integer;
- the ratio between the number of teeth and velocity ratio i should ensure allowable accuracy $\pm\Delta i$;
- without any additional conditions, a planetary gear unit should have zero teeth (gear $z \geq z_{min} = 17$, internal gear $z \geq z_{min} = 85$);
- axis of central gear of a planetary gear unit should conform to the axis of carrier to ensure coaxial allocation;
- if satellites are allocated in the same plane without eccentricity, two nearby satellites should have a gap between them. Size of gap can be calculated using the following formula (3) [9]:

$$2r_H \cdot \sin\left(\frac{\pi}{k}\right) > (d_{cam})_{max} \Rightarrow \sin\left(\frac{\pi}{k}\right) > \frac{z_2+2}{z_1+z_2}, \quad (3)$$

where $d_{a_{cam}} = m(z_2 + 2)$ – tip diameter of satellite.

- f. in the case of many satellites, assembly should be done without effort with equal radial pitch of teeth (formula (4)) [9]:

$$\frac{z_1 \cdot i_{1H}}{k} (1 + kp) = C, \quad (4)$$

where z_1 – the number of central gear teeth;

i_{1H} – the velocity ratio of entering stage 1 and output stage H;

k – the number of satellites;

$C = 1, 2, 3, \dots$ – integer, $p = 0, 1, 2, \dots$ – integer.

Allowable bending stress of nitrided steel 41CrMo (formula (5)) [9]:

$$[\sigma_F] = \left(\frac{\sigma_{Flim}^0}{S_F} \right) Y_R K_{FL} K_{FC} = 770 \text{ MPa}, \quad (5)$$

where $\sigma_{Flim}^0 = 700 \text{ MPa}$ – the allowable stress of material;

S_F – the safety factor;

Y_R – the tooth surface roughness factor;

K_{FL} – the longevity factor;

K_{FC} – the double-faced load factor.

Maximum allowable stress (formula (6)) (see Table 5, Fig. 7) [9]:

$$\sigma_{F1} = Y_{F1} \frac{F_{t1}}{b_1 \cdot m} K_{F\beta1} K_{F\vartheta1} = 233 \text{ MPa}, \quad (6)$$

where Y_{F1} – the tooth form factor;

$K_{F\beta1}$ – the concentrator factor;

$K_{F\vartheta1}$ – the dynamic factor.

Table 5

Maximum Allowable Stress

Stage	Number of gear teeth (z)		$\frac{z_1 \cdot i_{1H}}{k} (1 + kp) = C$	Max stress, MPa
1st stage	6	36	168	64
	4	90		
	5	27		130
2nd stage	1	60	232	233
	3	114		
	2	27		512

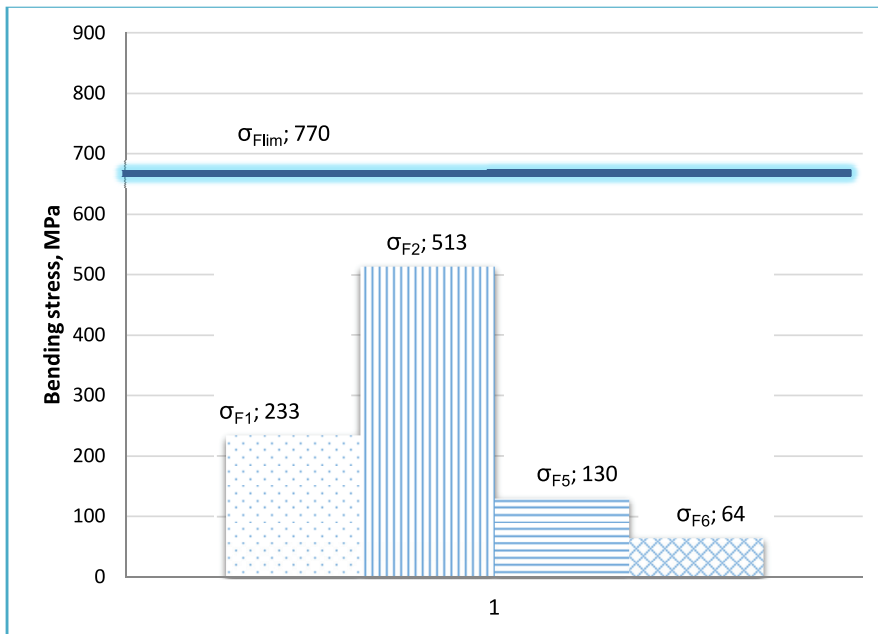


Fig. 7. Planetary gear unit bending stress.

6. CONCLUSIONS

The development of experimental planetary gear unit allowed making several tests and obtaining results that comply with theoretical calculations. After kinematic and load analysis as well as control of rotation frequency, it is possible to declare that the designed unit is able to operate at designated quality. Theoretical calculations and test results obtained were used for industrial WT prototype development.

ACKNOWLEDGEMENTS



The present research has been supported by the European Regional Development Fund within the project “Development of Industrial Prototype of Innovative Vertical Rotation Axis Wind Turbine for Performing the Tasks of Latvian National Economy” No. 2DP/2.1.1.1./13/APIA/VIAA/011

REFERENCES

1. Betz, A. (1966). *Introduction to the Theory of Flow Machines* (D. G. Randall, Trans.) Oxford: Pergamon Press.
2. Intergovernmental panel on climate change (2015). *IPCC Special Report on Emissions Scenarios*. Available at <http://www.grida.no>
3. Fateev, E.M. (1948). *Vetrodvigateli i vetroustanovki*. Moscow: OGIZ.

4. Jamieson, P. (2011). *Innovation in Wind Turbine Design (1)* (E-book). Wiley & Sons, Incorporated.
5. Lyatkher, V. (2013) *Wind Power: Turbine Design, Selection, and Optimization (1)* (E-book). Wiley & Sons, Incorporated.
6. National Research Council. (1991). *Assessment of Research Needs for Wind Turbine Rotor Materials Technology*. Washington: National Academies Press.
7. Rodionov, V. (2010). *Problemy nastojashhego i vozmozhnosti budushhego*. Moscow: JeNAS.
8. Shefter, Ja.I., & Rozhdestvenskij, I.V. (1957). *Izobretatelju o vetrodvigateljah i vetroustanovkah*. Minsk: Syel'skogo Hoz-va SSSR.
9. Urbahs, A., Krinicins, A., & Simanovskis, E. (2000). *Zobratu pārvadu aprēķins un konstruēšana*. Rīga: RTU.
10. Urbahs, A., Ribickis, L., & Scavinskis, R. (2010). Wind powered engine. LV patent No. LV14060.
11. Urbach, A., Banov, M., Turko, V., & Tsaryova, K. (2012). The characteristic features of composite materials specimen's static fracture investigated by the acoustic emission method. *Applied Mechanics and Materials*, 232, pp. 28-32.

VĒJA ENERĢĒTISKĀS IEKĀRTAS PLANETĀRA REDUKTORA EKSPERIMENTĀLA PROTOTIPA IZSTRĀDE UN NOVĒRTĒŠANA

A.Urbahs, M.Urbaha, K.Carjova

K o p s a v i l k u m s

Rakstā doti vēja enerģētiskās iekārtas (VEI) planetārā reduktora matemātiskie aprēķini un eksperimentālo pētījumu rezultāti. No kompozītmateriāliem tika izveidoti divi VEI planetārā reduktora eksperimentālie prototipi (mēroga modeļi). Lai iegūtu planetārā reduktora raksturlielumus, tika izmantots Holla devējs, servomehānismi un optiskais tahometrs. Pēc tam tika veikta iegūto datu un teorētisko aprēķinu salīdzinošā analīze. Kinemātiskā un slodžu analīze, kā arī rotācijas frekvences kontroles testi pierādīja eksperimentālo prototipu efektivitāti. Iegūtie rezultāti tika izmantoti VEI industriālā prototipa izstrādei.

26.06.2017.

DOI: 10.1515/lpts-2017-0034

GRID STUDY ON THE BASIS OF ALLOCATED
POWER LOSS CALCULATION

J. Survilo

Riga Technical University,
12 Azenes Str., Riga, LV-1048, LATVIA

Studying the loss allocation, it is possible to determine the loss which appears in some grid section or line (allocated power loss) as a result of: 1) some power source sending its power to the consumers, 2) some power source sending its power to a certain power consumer, 3) power received by some consumer. Determining allocated power losses, it happens that some of them are negative. It turned out that this phenomenon is not rare and appears at a definite power distribution between suppliers. Negative allocated power loss shows that total power loss is increased. Computing the allocated loss, the possibility appears to define other grid quantities that characterize grid properties and operation, as well as to find out those suppliers and consumers who mainly affect the grid operation.

Keywords: *loss allocation, node voltage, power losses, voltage drop*

1. INTRODUCTION

Attention to power losses has been drawn at the very beginning of electricity use. Losses were considered in the grid or on specified territory without being tied to a particular source of electricity or to the consumer, for example, in [1]. Optimizing the grid in order to reduce active power losses is considered in [2] without calculating the losses attributed to a particular power plant. With the deregulated work of the power system, it became necessary to determine the losses incurred by a particular power system subject – power supplier or consumer, but neither [1] nor [2] considered allocated power losses (AL) because there were other problems to be dealt with. Let us dwell on the literature which treats the issue in the light of new requirements to the operation of power systems. Extensive literature appeared on the topic of (AL). The question is solved in two directions. Topographic direction proposed by J. Bialek [3] is based on tracing the currents. The methods of this direction [4] take a lot of work even after a tedious job is made to trace the currents in all lines is made. In analytical direction, issue is solved by matrix algebra [5]. The complicated algorithm gives a possibility to calculate the quantities (node voltages, the angles and so on) which can be given by any load flow program. To calculate the load loss allocation, it is not necessary to derive such complex expressions [6]. Both directions do not provide a simple and uniform algorithm for any grid configuration.

The procedure which allows finding the AL transmitting the electricity from a specified supplier to a certain consumer is called here a double algorithm (DA). This procedure is most fully described in [7], [8]. The DA is based on two computer programs: power flow program (more appropriate is Power World) and Matlab. The main part of the work connected with the configuration of the grid takes over power flow program. The DA has an advantage that it is apt for all grid configurations, radial grids and closed grids. Computing by the DA, the joint current (JC), AL and other extra quantities are defined. JC is current that originates in some source or supplier and, flowing in some place of a grid, flows to a certain consumer.

Making practical estimates in [8] for a closed grid, it appeared that some AL could be negative. The question arises: can negative AL be in radial grids as well; what is the reason? Moreover, computing AL by the DA, the extra (secondary) quantities and properties can be defined, which can be applied to in-depth grid characteristics. The goal of the paper is to clarify negative AL, extra quantities and properties.

Radial Q (Fig. 1 a) and closed F (Fig. 1 b) 330 kV grids are investigated. Different cases of each scheme with dissimilar loads are computed by the DA (Table 1), altogether 20 cases.

The units A, V, VA, W are used if other is not indicated.

2. SECONDARY QUANTITIES

AL is an initial quantity searched for by the DA. Applying the DA, some other quantities can be defined, which help to evaluate a grid in a versatile manner.

One of them is joint impedance (JI). For example, between supplier 4 and consumer 1 (Fig. 1 a) the JI Z_{4t1} can be calculated using the formula:

$$Z_{4t1} = \Delta s_{4t1} / |I_{4t1}|^2, \quad (1)$$

where Δs_{4t1} is AL, I_{4t1} – JC transmitting the power from supplier 4 to consumer 1.

Some of JI for case Qa are: $Z_{4t1}=28+49i$; $Z_{4t6}=59+191i$; $Z_{5t1}=-12-120i$; $Z_{5t3}=-74-238i$; $Z_{7t1}=4.8+19.7i$. For case Fa: $Z_{4t1}=113+741i$; $Z_{4t2}=21+141i$; $Z_{5t2}=17+108i$; $Z_{7t3}=-49-249i$. Negative AL has negative JI. At small changes of node current values, JI can be used for quick estimation of AL.

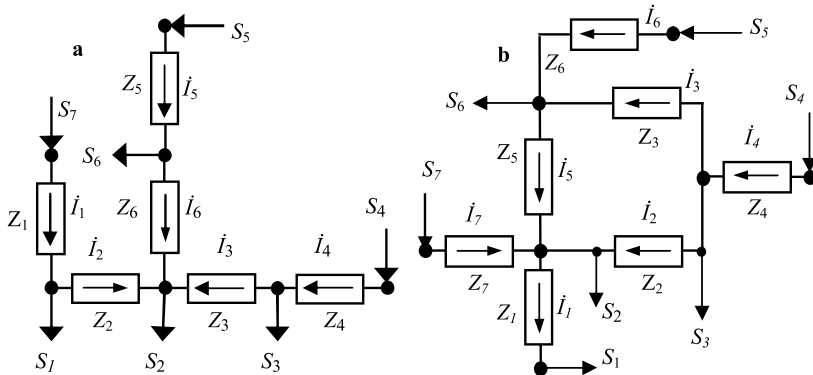


Fig. 1. 330 kV grid circuit diagrams

S_4, S_5, S_7 are flows to power supplying points; S_1, S_2, S_3, S_6 – flows to consumers; I – branch currents;

Z – transmission line impedances. Branch numbers coincide with impedance indices, node numbers – with power S indices; node currents J (not shown) correspond to node flows S . All shown quantities are complex numbers.

a – radial grid Q: $Z_1=0.785+3.2i$, $Z_2=5.58+28.8i$, $Z_3=7.425+24i$, $Z_4=1.782+5.76i$, $Z_5=3.465+11.2i$, $Z_6=3.366+10.88i \Omega$;

b – closed grid F: $Z_1=11.22+70.4i$, $Z_2=6.1+32i$, $Z_3=6.48+25.6i$, $Z_4=11.125+80i$, $Z_5=1.02+6.4i$, $Z_6=10.2+64i$, $Z_7=0.81+3.2i \Omega$.

Table 1

List of Comuted Cases and Node Flows, MVA

Case	S_1	S_2	S_3	S_4	S_5	S_6	
MVA							
Qa	40	160+30 <i>i</i>	20+10 <i>i</i>	100+14 <i>i</i>	50+5 <i>i</i>	30+3 <i>i</i>	
Qc				75+8.5 <i>i</i>	75+8.5 <i>i</i>		
Qc1				60+6.8 <i>i</i>	90+10.2 <i>i</i>		
Qc2				67.5+7.65 <i>i</i>	82.5+9.35 <i>i</i>		
Q2i		208+39 <i>i</i>		100+14 <i>i</i>	50+5 <i>i</i>		
Q2i3		256+48 <i>i</i>					
Q2r		100+100 <i>i</i>					
Q4i3		160+50 <i>i</i>					
Q4r			70+60 <i>i</i>				
Fa			100+14 <i>i</i>	40			
Fc		56+5.6 <i>i</i>	84+8.4 <i>i</i>				
Fc1		42+4.2 <i>i</i>	58+5.8 <i>i</i>				
Fc2		25.8+2.58 <i>i</i>	34.2+3.42 <i>i</i>				
Fc3		18.48+1,848 <i>i</i>	23.52+2.352 <i>i</i>				
Fc4		12.43+1.243 <i>i</i>	15.57+1.57 <i>i</i>				
Fc5		15.68+1.568 <i>i</i>	19.32+1.93 <i>i</i>				
F2d		50+20 <i>i</i>	100+14 <i>i</i>	40			
F2r		40+100 <i>i</i>					
F4w6		160+30 <i>i</i>	0				
F4w4			50+7 <i>i</i>				

Partial losses of any partial current in any power line can be computed. Any current out of more of them which all flow in some grid section is called here partial current. JC is partial current as well.

For example, in the case Qa, losses $\Delta S_{2,J_{40}}$ caused by the current $I_{2,J_{40}}$ ($I_{2,J_{40}}$ is the part of node 4 current that flows in branch 2) in branch 2 are

$$\Delta S_{2,J_{40}} = (1/4)Z_2(|I_2 + I_{2,J_{40}}|^2 - |I_2 - I_{2,J_{40}}|^2), \quad (2)$$

where I_2 is summary current which flows in line 2. Formula (2) is explained in Section 6.

Computed loss value is $\Delta s_{2/40} = -16094 - 83065i$; although AL $\Delta s_{4/1}$ is positive (see Table 2), supplier 4 reduces it in line 2. This can be taken into account when financing the line reconstruction.

Similarly, power losses in line 2 of JC flowing from supplier 4 to consumer 1 ($I_{2/41}$) can be computed as follows:

$$\Delta s_{2/41} = 0.25 Z_2 (|I_2 + I_{2/41}|^2 - |I_2 - I_{2/41}|^2). \quad (3)$$

Loss value is $\Delta s_{2/41} = -16094 - 83064i$, it is equal to loss $\Delta s_{2/40}$ since $I_{2/40} = I_{2/41}$. Loss $\Delta s_{5/50} = 27263 + 88121i$, and $\Delta s_{5/51} = 4164.2 + 13460i$ since $I_{5/50} \neq I_{5/51}$.

Voltage drop across a line from partial current is a linear function of this current, e.g., voltage drop across line 2 from JC in line 2 $I_{2/41}$ (see above) is

$$\Delta u_{2/41} = Z_2 I_{2/41} \quad (4)$$

and is equal to $-133-791i$; this voltage drop is negative because in Fig. 1a current $I_{2/41}$ flows in the opposite direction. This quantity shows which partner pair causes voltage deviations in a grid.

3. NEGATIVE ALLOCATED POWER LOSSES

Cases Qa and Fa are used to deal with the negative losses.

Table 2 shows that radial scheme Qa has even three negative AL. Closed scheme Fa has only one – from supplier 7 to consumer 3.

To find the reason of negative AL, let us calculate AL in case Qa by transmitting electricity from supplier 5 to consumer 3, namely $\Delta s_{5/3}$. For clarity reason, this is done without the use of matrix algebra formulas. Current values computed by the DA are used. JC $I_{5/3}$ flows in impedances Z_3, Z_5, Z_6 : $I_{3/53} = -7.0907 + 3.0637i$; $I_{5/53} = 7.0907 - 3.0637i$; $I_{6/53} = 7.0907 - 3.0637i$. JC $I_{5/3}$ or its portions do not flow in the impedances Z_1, Z_2, Z_4 . Total currents in the impedances with JC $I_{5/3}$ are $I_3 = 140.47 - 6.09i$; $I_5 = 88.16 - 9.77i$; $I_6 = 35.18 - 3.63i$. The AL $\Delta s_{5/3}$ is the sum of partial losses in impedances Z_3, Z_5, Z_6 . Computing by formulas of the type (3), we have: $\Delta s_{3/53} = 0.25 Z_3 (|I_3 + I_{3/53}|^2 - |I_3 - I_{3/53}|^2)$; $\Delta s_{5/53} = 0.25 Z_5 (|I_5 + I_{5/53}|^2 - |I_5 - I_{5/53}|^2)$; $\Delta s_{6/53} = 0.25 Z_6 (|I_6 + I_{6/53}|^2 - |I_6 - I_{6/53}|^2)$.

These currents in the impedances give loss values: $\Delta s_{3/53} = -7534.062 - 24352.524i$; $\Delta s_{5/53} = 2269.1769 + 7334.7132i$; $\Delta s_{6/53} = 877.08535 + 2835.2325i$, which being summed amount to $\Delta s_{5/3} = -4387.8 - 14182.578i$. This value almost does not differ from the one calculated by the DA (see Table 2). The loss in impedance Z_3 is of great negative value which exceeds the sum of the positive values of the rest two impedances. It is negative because JC $I_{3/53}$ is directed against total current I_3 . Thus a precondition of negative AL existence is that of opposite direction of total current and JC. However, the summary result depends on other currents and impedances.

In closed grids F, there is only one negative AL. Here the path between two partners (between a supplier and a consumer) ramifies, opposite directed currents are smaller and they are less. Total grid power losses are always greater when at some

partner pair or in any grid branch negative losses appear. An absolute value of negative AL is less than the increment of positive losses at other partner pair. In a closed grid, this phenomenon is less pronounced.

To present negative losses as a result of equalizing currents, the appropriate mathematical expressions are necessary.

Table 2

RL on the Path from Supplier 4,5,7 to Consumer 1, 2, 3, 6

Case	Consumer	supplier 4 $\Delta s_{4l1,2,3,6}$	supplier 5 $\Delta s_{5l1,2,3,6}$	supplier 7 $\Delta s_{7l1,2,3,6}$
Qa	1	20934+36622i	- 2195-22479i	4086+16658i
	2	154210+498440i	24360+78740i	93347+463380i
	3	4851+15681i	- 4387-14181i	- 1868+15691i
	6	26081+84302i	3270+10570i	14449+76158i
Fa	1	92800+609230i	18155+114630i	28654+169110i
	2	286120+1905100i	37304+237040i	18750+74074i
	3	13868+99726i	758+7274i	- 868-14510i
	6	51199+340240i	6186+38814i	1585+442i

4. SUPPLIER OPTIMAL USE

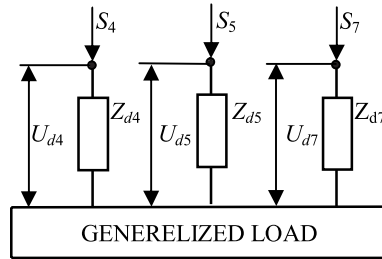


Fig. 2. Representation of the grid with the view of optimization.

Total grid power losses depend on distribution of power (which is necessary for consumers) between suppliers. If electricity price of all suppliers is the same, the farther a supplier is located from consumers the less electricity should be purchased from him due to increased losses. Optimal power distribution comes on when active components of the distinctive voltages U_d across the path from a supplier to a generalized load (Fig. 2) are equal for all suppliers.

Distinctive voltages can be defined by the following formulas:

$$U_{d4} = \Delta s_4 / |J_4|; U_{d5} = \Delta s_5 / |J_5|; U_{d7} = \Delta s_7 / |J_7|, \quad (5)$$

where $\Delta s_4, \dots, \Delta s_7$ are power losses caused by suppliers 4; 5; 7. Those are supplier losses:

$$\Delta s_4 = \Delta s_{4t1} + \Delta s_{4t2} + \Delta s_{4t3} + \Delta s_{4t6}; \Delta s_5 = \Delta s_{5t1} + \dots; \Delta s_7 = \Delta s_{7t1} + \dots \quad (6)$$

The less active components of distinctive voltages vary, the smaller active total power losses are. This is illustrated by the following. Distinctive voltages computed for case Qa are $U_{d4}=1163+3583i$, $U_{d5}=237+594i$, $U_{d7}=600+3120i$, grid power loss is $\Delta p=337130$. For case Fa, the values are $U_{d4}=2562+17048i$, $U_{d5}=894+5696i$, $U_{d7}=248+1233i$, $\Delta p=552510$. To find out a better option with smaller grid losses, the cases Qc, Qc1, Qc2, Fc, Fc1, Fc2, Fc3, Fc4, Fc5 were computed until a better load distribution option was found. Grid Q has a better case Qc2: $U_{d4}=650+1929i$, $U_{d5}=643+1906i$, $U_{d7}=616+3179i$, where $\Delta p=285161$; closed grid – case Fc5: $U_{d4}=463+3128i$, $U_{d5}=464+2921i$, $U_{d7}=427+1993i$, $\Delta p=183942$. Nevertheless, negative AL quickly disappear when active components of distinctive voltages drop.

Distinctive impedances which are defined as:

$$Z_{d4} = \Delta s_4 / |J_4|^2; Z_{d5} = \Delta s_5 / |J_5|^2; Z_{d7} = \Delta s_7 / |J_7|^2, \quad (7)$$

vary relatively little when the load changes. For example, in a radial grid, the loads of cases Qa and Qc vary (see Table 1), but distinctive impedances for case Qa are: $Z_{d4}=6.56+20.21i$; $Z_{d5}=2.68+6.69i$; $Z_{d7}=3.37+17.02i$; for case Qc2: $Z_{d4}=5.43+16.1i$; $Z_{d5}=4.4+13.04i$; $Z_{d7}=3.35+17.3i$. In a closed grid, they are still closer.

It seems that supplier losses are approximately proportional to supplier current square.

5. FAST DETERMINATION OF NODE VOLTAGES

It goes without saying that if the supplier or consumer power changes, voltage in all grid nodes changes as well. Node sensitivity to power change depends on how far electrically one node is located from the other.

To determine this sensitivity, two modes (cases) should be computed: the first most common (base) mode where node phase voltages U_{vib} are found. Cases Qa and Fa are taken as base ones. Computing the second (auxiliary) mode, node phase voltages U_{via} are obtained, where i is node number, b and a denote base and auxiliary mode. Using these voltages, conjoint sensitivity of the nodes can be found. On the basis of these calculations, it can be fast determined what awaits each node by load or supply power change at any other node. Node voltages can be computed by any appropriate program as well, but the proposed method makes it possible to survey the situation at all nodes at once without using the computer program.

The circuit diagram in Fig. 3a illustrates the said. A grid can be deemed as an assemblage of voltage sources [9]. It can be represented by its no-load voltages U_{vib} in base mode (i stands for $1 \dots 6$, b – for basic) and by putative impedances. Slack bus voltage U_{v7} here is not topical. Figure 3a shows putative impedances $Z_{4p1}, \dots, Z_{4p3}, Z_{4p5}, Z_{4p6}$; they are internal impedances of voltage source for related influenced node and are fit only when current changes at influencing node of supplier 4. Z_{4s} is putative impedance of influencing node 4.

If power at influencing node 4 does not change ($\Delta J_4=0$), eventual voltages U_{v1e}, \dots, U_{v6e} at all 1, ..., 6 nodes do not change and they are U_{v1b}, \dots, U_{v6b} . When power at influencing node changes ($\Delta J_4 \neq 0$), to determine eventual voltage, e.g., U_{v3e} at node 3 (or U_{v4e} at node 4), it is necessary to move the contact of switch S to impedance Z_{4p3} (or Z_{4s}). Then eventual voltage at node 3 (or 4) is

$$U_{v3e} = U_{v3b} + Z_{4p3} \Delta J_4; \quad U_{v4e} = U_{v4b} + Z_{4s} \Delta J_4. \quad (8)$$

Eventual voltages at other influencing nodes are calculated in the same way. In Fig. 3b, the influencing node is consumer node 2.

Putative impedances of supplying nodes are positive, but those of consumer nodes are negative. They are defined by formulas:

$$Z_{ipk} = \frac{U_{vka} - U_{vkb}}{J_{ia} - J_{ib}}; \quad Z_{is} = \frac{U_{via} - U_{vib}}{J_{ia} - J_{ib}}, \quad (9)$$

where U_{vka} and U_{vkb} are voltage of influenced node k in auxiliary and base modes; J_{ia} and J_{ib} is the current of influencing node i in auxiliary and base modes, which are obtained by the DA; U_{via} and U_{vib} – respective voltages of influencing node (Table 3). The computed putative impedances for auxiliary case Q2i (base mode being Qa) are: $Z_{2p1} = -0.924-3.257i$; $Z_{2s} = -5.667-31.652i$; $Z_{2p3} = -5.096-31.569i$; $Z_{2p4} = -4.875-31.505i$; $Z_{2p5} = -5.466-31.648i$; $Z_{2p6} = -5.641-31.653i$. The closer the influenced node is to the influencing one, the greater is putative impedance (its absolute value), it is the greatest one for influencing node Z_{is} itself.

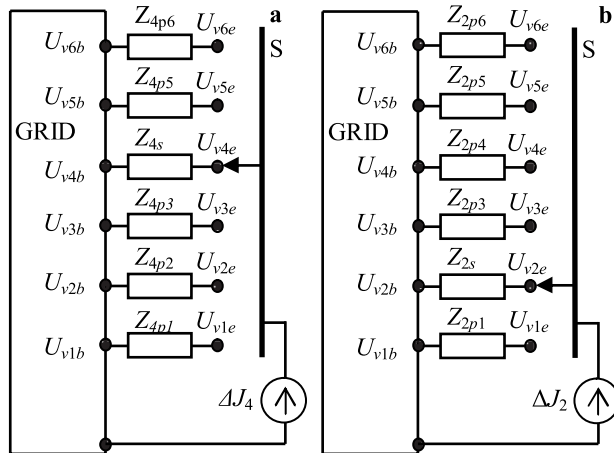


Fig.3. Updating the voltage in a grid

a – change ΔJ_4 (at node 4) of supplier current,

b – change ΔJ_2 (at node 2) of consumer current.

Table 3

Main Mode Data of Cases Qa and Q2i

Node	Base case Qa		Auxiliary case Q2i	
	J	U_v	J	U_v
1	70.09-0.2i	190234.4-521.7i	70.14-0.29i	190080 - 780i
2	282.29-58.10i	188245.9-3322.9i	368.15-81.14i	187030 - 5910i
3	35.19-17.60i	189435+3.1i	35.16-18.19i	188270 - 2590i
4	175.66-23.69i	189884.5+972.7i	176.39-26.24i	188740 - 1620i
5	88.16-9.77i	188818.6-1998.7i	88.56-11.05i	187620 - 4590i
6	52.98-6.14i	188403.7-2952.3i	53.22-6.92i	187190 - 5540i
7	176.73-48.58i	190528.6+5.7i	261.71-69.21i	190510

In eventual (updated) mode, voltages U_{vke} of influenced and U_{vie} of influencing modes are

$$U_{vke} = U_{vkb} + Z_{ipk}(J_{ie} - J_{ib}); \quad U_{vie} = U_{vib} + Z_{is}(J_{ie} - J_{ib}). \quad (10)$$

This time the current J_{ie} of influencing node in eventual mode is not computed by the DA or by any other program because it is embarrassing; it is calculated using known voltage U_{vib} and changed (eventual) power S_{ie} of node i :

$$J_{ie} = \frac{\hat{S}_{ie}}{3\hat{U}_{vib}}. \quad (11)$$

If there is doubt about accuracy, the calculation of eventual current J_{ie} of node i can be repeated, using voltage U_{vie} calculated by formula (10):

$$J_{ie}^{(1)} = \frac{\hat{S}_{ie}}{3\hat{U}_{vie}}. \quad (12)$$

In the paper, eventual mode is computed by the DA as well. It is done in order to check the accuracy of the method, voltages U_{vkeDA} and U_{vieDA} are obtained. The accuracy d_k ; d_i is defined as voltage difference between node voltages obtained by fast method (U_{vke} ; U_{vie}) and by the DA (U_{vkeDA} ; U_{vieDA}); this difference is related to the true voltage difference (the difference between eventual obtained by the DA (U_{vkeDA} ; U_{vieDA}) and base voltages (U_{vkb} ; U_{vib}):

$$d_k = \frac{|U_{vke} - U_{vkeDA}|}{|U_{vkeDA} - U_{vkb}|}; \quad d_i = \frac{|U_{vie} - U_{vieDA}|}{|U_{vieDA} - U_{vib}|}. \quad (13)$$

Accuracy values for some cases are shown in Table 4. The accuracy is better when node power angle of all three modes is closer (see Table 1).

Table 4

Accuracy of Node Voltages

Case			d_{1e}	d_{2e}	d_{3e}	d_{4e}	d_{5e}	d_{6e}
basic	auxil.	event.	$d_{1e}^{(1)}$	$d_{2e}^{(1)}$	$d_{3e}^{(1)}$	$d_{4e}^{(1)}$	$d_{5e}^{(1)}$	$d_{6e}^{(1)}$
Qa	Q2i	Q2i3	0.0460	0.0771	0.0765	0.0780	0.0756	0.0757
			0.0577	0.0053	0.0018	0.0021	0.0040	0.0052
Qa	Q2i	Q2r	0.0981	0.0188	0.0375	0.0472	0.0226	0.0197
			0.0576	0.0472	0.0759	0.0864	0.0578	0.0496
Qa	Q4i3	Q4r	0.0337	0.0602	0.0261	0.0215	0.0488	0.0744
			0.0856	0.0112	0.0732	0.0661	0.0960	0.0439
Fa	F2d	F2r	0.0332	0.0102	0.0193	0.0969	0.0331	0.0115
			0.0299	0.0098	0.0214	0.0995	0.0357	0.0120
Fa	F4w6	Fw4	0.0459	0.0461	0.0454	0.0453	0.0467	0.0460
			0.0009	0.0031	0.0021	0.0021	0.0047	0.0071

$d_{1e}^{(1)}, d_{2e}^{(1)}, \dots$ is accuracy, obtained using node currents $J_{1e}^{(1)}, J_{2e}^{(1)}, \dots$.

6. CLARIFICATION OF TWO FORMULAS

1) In referred publications, using the DA algorithm, node currents \dot{J} are defined as

$$J_i = \frac{\hat{S}_i}{\sqrt{3}\hat{U}_i}, \quad (14)$$

where \hat{S}_i and \hat{U}_i are conjugate values of node power and line voltage \dot{U}_{ab} . Since phase voltage \dot{U}_{ph} is shifted by 30° [11], it should be

$$J_i = \frac{\hat{S}_i}{\sqrt{3} \cdot \text{conj}(\dot{U}_i e^{-j30^\circ})}. \quad (15)$$

However in expression (14), there is no error because PowerWorld program gives phase-to-phase voltage with phase voltage angle.

2) Based on [10]; [7]; [8], power loss in impedance Z with currents $I = I_1 + I_2 + \dots + I_n$ (Fig. 4) from any of currents (for example, from current I_2 power loss Δs_2) can be defined by expression:

$$\Delta s_2 = k \frac{Z}{4} \left(\left| \dot{I} + \frac{\dot{I}_2}{k} \right|^2 - \left| \dot{I} - \frac{\dot{I}_2}{k} \right|^2 \right) = \frac{1}{\kappa} \frac{Z}{4} \left(\left| \dot{I} + \kappa \dot{I}_2 \right|^2 - \left| \dot{I} - \kappa \dot{I}_2 \right|^2 \right); \quad \kappa = \frac{1}{k}. \quad (16)$$

The substitution $\kappa=1/k$ is made for convenience in further consideration.

For example, if $k=100$, then $\Delta s_2 = 25Z(|\dot{I} + 0.01\dot{I}_2|^2 - |\dot{I} - 0.01\dot{I}_2|^2)$, (see [6]).

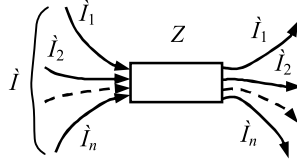


Fig. 4. Branch Z with several currents.

Complex numbers can be represented as:

$$\dot{I} = I(\cos \alpha + j \sin \alpha); \quad \dot{I}_2 = I_2(\cos \beta + j \sin \beta). \quad (17)$$

Inserting (17) in expression $|\dot{I} + \kappa\dot{I}_2|^2 - |\dot{I} - \kappa\dot{I}_2|^2$ we obtain (18) and inserting (18) in equation (16), we obtain (19):

$$|\dot{I} + \kappa\dot{I}_2|^2 - |\dot{I} - \kappa\dot{I}_2|^2 = 4\kappa I I_2 [\cos(\alpha - \beta)] = 4\kappa I I_2 (\cos \alpha \cos \beta + \sin \alpha \sin \beta); \quad (18)$$

$$\Delta s_2 = Z I I_2 (\cos \alpha \cos \beta + \sin \alpha \sin \beta). \quad (19)$$

Whatever k (or $\kappa=1/k$) we introduce into (16), we still get (19). When we assume $k=1$, we see a simpler formula similar to expressions (2) and (3):

$$\Delta s_2 = 0.25Z(|\dot{I} + \dot{I}_2|^2 - |\dot{I} - \dot{I}_2|^2). \quad (20)$$

The decrease in k times of partial current (it was conjoint current) was necessary in the very beginning [10] when AL was looked for.

The sum of partial losses, obtained on the basis of expressions (16) and (20), is equal to the loss of summary current which corresponds to the meaning of electrical engineering.

The author of the research does not know any formula of a different type where the sum of partial losses is equal to the summary current losses.

7. CONCLUSIONS

1. Partial power losses and partial voltage drops can be computed for each grid branch, this allows fixing the source of hard mode in the grid.
2. Negative AL indicate a particular market partner pair; they signify that total grid power losses are increased. Negative AL can appear when JC in some branch is directed opposite to the total current of this branch.
3. In the grid with minimal power losses, values of active components of distinctive voltages for all suppliers are equal or close.
4. Using putative impedances and node voltage levels, the grid response to power changes can be surveyed.

REFERENCES

1. Казанцев, В. (1983). *Методы расчета и пути снижения потерь энергии в электрических сетях*. Свердловск: Издание УПИ, pp. 10 – 68.
2. Gerhards, J., Mahnitko, A., & Papkovs B., (2011). *Energosistēmas vadība, optimizācija un riski*. Rīga: RTU, pp. 78 – 84.
3. Bialek, J. (1996). Tracing the Flow of Electricity. In *IEEE Proceedings on Generation, Transmission and Distribution*, 143(4), 313-320.
4. VinothKumar, M. & Arul, P. (2013). *Power Tracing and Loss Allocation in a Power System by Using Bialek's Algorithm*. Available at ijettjournal.org/volume-4/issue-10/IJETT-v4I10P108.pdf.
5. Teng, J.-H. (2005). *Power Flow and Loss Allocation for Deregulated Transmission Systems*. Available at [opac.vimaru.edu.vn/edata/E-Journal/2005/International journal of electric power and energy system/ issue4/bai9.pdf](http://opac.vimaru.edu.vn/edata/E-Journal/2005/International%20journal%20of%20electric%20power%20and%20energy%20system/issue4/bai9.pdf).
6. Gross, G. & Shu Tao. (1998). A Loss Allocation Mechanism for Power System Transactions. In *Proceedings of Bulk Power System Dynamics and Control IV – Restructuring*, August 24-28, Santorini, Greece. Available at: gross.ecce.illinois.edu/.../1998-Aug-A-Loss-Allocation-Mechanism-for-...
7. Survilo, J. (2014). Determination of Reciprocal Current by Electricity Delivery to More than One Consumer. In *Proceedings of the 55th International Scientific Conference of RTU*. Riga, Latvia.
8. Survilo, J. (2015). A Method for Node Prices Formation. In *Proceedings of the 56th International Scientific Conference of RTU*. Riga, Latvia.
9. Нейман, Л., Демирчян, И. (1967). *Теоретические основы электротехники. Часть первая*. Ленинградское отделение издательства “Энергия”, pp. 135, 136.
10. Survilo, J. (2013). Reciprocal load-generator power losses in a grid. *Latv. J. Phys. Tech. Sci*, 6, 48-53.
11. *The voltages in the three-phase power are produced by a system ...* Available at www.my.ece.msstate.edu/faculty/.../ece3614tkree_phase_power.pdf.

TĪKLU PĒTĪJUMI UZ SAVSTARPĒJO ZUDUMU APRĒĶINU BĀZES

J. Survilo

Kopsavilkums

Nosakot saistītos jaudas zudumus (zudumus, kas rodas pārvadot jaudu no kāda piegādātāja kaut kādam patērētājam) tīklā, gadās, ka daži saistītie zudumi ir negatīvi. Izrādījās, ka šī parādība nav reta un rodas pie noteiktas piegādātāja jaudas sadales. Negatīvie saistītie zudumi uzrāda, ka ir palielināti kopējie jaudas zudumi tīklā. Aplēšot zudumus, ir iespēja noteikt citus tīkla lielumus, kuri raksturo tīkla īpašības un darbu, kā arī ļauj noskaidrot tos piegādātājus un patērētājus, kuri ietekmē tīkla darbu.

26.09.2016.

EVALUATION OF SIGNAL REGENERATION IMPACT ON THE POWER EFFICIENCY OF LONG-HAUL DWDM SYSTEMS

D. Pavlovs, V. Bobrovs, M. Parfjonovs, A. Alsevska, G. Ivanovs

Institute of Telecommunications, Riga Technical University

12 Azenes Str., Riga, LV-1048, LATVIA

Due to potential economic benefits and expected environmental impact, the power consumption issue in wired networks has become a major challenge. Furthermore, continuously increasing global Internet traffic demands high spectral efficiency values. As a result, the relationship between spectral efficiency and energy consumption of telecommunication networks has become a popular topic of academic research over the past years, where a critical parameter is power efficiency.

The present research contains calculation results that can be used by optical network designers and operators as guidance for developing more power efficient communication networks if the planned system falls within the scope of this paper. The research results are presented as average aggregated traffic curves that provide more flexible data for the systems with different spectrum availability. Further investigations could be needed in order to evaluate the parameters under consideration taking into account particular spectral parameters, e.g., the entire C-band.

Keywords: *differential phase shift keying, DWDM, energy efficiency, optical fibre networks, phase shift keying, power consumption, power efficiency, single-line rate, spectral efficiency, sub-band spacing, WDM networks*

1. INTRODUCTION

The Information and Communication Technology (ICT) sector is experiencing continuously increasing global Internet traffic due to emergence and establishment of bandwidth-intensive applications (e.g., IPTV, YouTube, and cloud computing) [1]. Recent Cisco study has shown that the total IP traffic increases annually by an average of 23 % for 2014–2019. The increased traffic raised the necessity of updating the existing transmission techniques and developing new ones in order to enhance spectral efficiency of systems.

In terms of wavelength division multiplexing (WDM) systems, the system capacity can be increased by either 1) channel-spacing reduction (increase of the transmitted channel number), or by 2) enhancing of channel capacities. The mentioned relation can be expressed by equation (1) [2]:

$$C = \sum_i^M C_{ik} , \quad (1)$$

where i – the index number of channel; M – the number of transmission channels; C_{ik} – the speed of channel [bit/s].

However, higher spectral efficiency can result in the reduction of a transmission reach [3], [4]. Therefore in order to guarantee the required quality of transmission (QoT), an optical signal might require 3R (Re-amplification, Re-shaping, Retiming) regeneration procedure by means of optical-to-electrical-to-optical (OEO) conversion process, which in its turn requires the additional equipment in system nodes. As a result, the overall power consumption increases [5]. Thereby, it can be inferred that there is a trade-off among spectral efficiency, power consumption and transmission reach [1], [3], [4].

In the paper, the authors evaluate the impact of signal regeneration on power efficiency of a long-haul dense wavelength division multiplexing (DWDM) system by means of different channel spacing values, which is the most decisive factor for transmission reach of the system. This study aims at the single-line rate (SLR) solutions operating with 10 Gbps, 40 Gbps and 100 Gbps transmission signals with the most frequently used modulation formats in modern high capacity networks – non-return-to-zero on-off-keying (NRZ-OOK), non-return-to-zero differential phase-shift keying (NRZ-DPSK) and dual polarisation quadrature PSK (DP-QPSK), respectively. The calculations of power consumption have been performed for 2960 km transmission distance in order to achieve more pronounced regeneration influence. The present research focuses on the WDM systems with forward error correction (FEC), which by virtue of an error controlling technique, allows successfully demodulating transmitted signals when the bit error rate (BER) does not exceed 10^{-3} threshold. This setup allows taking into account power consumption contributed by the redundant data required for FEC technology, which is commonly used in modern transmission systems [6].

2. METHODOLOGY

For this study, the evaluation of system power consumption was performed in two steps. At first, the relation between BER level and channel spacing was defined on the fixed fibre length using OptSim™ simulation software in order to define transmission reach and its relation with the channel spacing for each considered system setup [7], [8]. The assignment of central channel wavelength was based on the ITU-T recommendation G.694.1. The recommendation also provides the nominal central frequency granularity, which is equal to 6.25 GHz. Therefore, the cross-channel interval was increased by 6.25 GHz at every simulation step with the purpose to find a frequency plan, whereby the BER level became lower than 10^{-3} . Further, based on the obtained data from the above-mentioned simulations the power consumption evaluation model was developed using MATLAB features. In the calculation code, the amount of transmitted data was defined as a variable, which was used to calculate

the required number of WDM components, which in conjunction with calculated transmission reach and chosen transmission distance determined the overall system power consumption. In this scenario, power consumption became a function of the transmitted data; therefore, calculation setup allowed evaluating power efficiency by dividing power consumption by the amount of transmitted data. The methodology was described in more detail in the previous papers [3] and [4].

For calculation purposes, the transmission distance was set for 2960 km, which is comparable with the longest node of National Science Foundation Network (NSFNET) – the US network used in many studies, i.e., [9] and [10].

It was assumed that the total power consumption of WDM system could be calculated using equation (2):

$$P_{WDM} = P_{ROADM} + P_{TRANS} + P_{WDMTERM} + P_{OLA} + P_{3R}, \quad (2)$$

where P_{WDM} – total power consumption of WDM system [W]; P_{ROADM} – power consumption of optical reconfigurable add/drop multiplexer [W]; P_{TRANS} – power consumption of transponder [W]; $P_{WDMTERM}$ – power consumption of WDM terminal [W]; P_{OLA} – power consumption of optical line amplifier [W]; P_{3R} – 3R (Re-amplification, Re-shaping, Re-timing) regenerator consumption [W].

Based on the provided datasheets and relevant studies [1], [4], [9], power consumption values of transponders and 3R regenerators are summarised in Table 1.

Table 1

Power Consumption [W] of Transponders and 3Rs

Bit Rate (Gbps)	Modulation format	Consumer	Power (W)
10	NRZ-OOK	TP/3R	34.0 (Typ.)
40	NRZ-DPSK	TP/3R	85 (Max)
100	DP-QPSK	TP/3R	139 (Typ.)

It should be noted that the equipment under normal operational conditions does not consume the declared maximal power. Therefore, for calculations the nominal power consumption accounted for 75 % of the specified maximal value.

Power consumption of ROADM multiplexers and WDM terminals, which are used for calculations, is demonstrated in Table 2 [1], [3], [9]. Power units of the optical line amplifier require 110W [3], [4], [9].

Table 2

ROADM and WDM Terminal Power Consumption [W]

Device	Power Consumption	
	40 ch. realisation	80 ch. realisation
WDM terminal	230	240
ROAD multiplexer	450	600

3. RESULTS AND DISCUSSION

In this section, the authors present the simulation results that show the relation between the consumed power by means of power efficiency and 3Rs' power ratio and the amount of transmitted information, with the view of providing more flexible data for different system realisations, i.e., a different number of transponders due to distinctions in the available spectrum.

With the aim to evaluate power efficiency and regeneration impact at different spectral efficiency states, different channel spacing values were set, based on the recommendation ITU-T G.694.1. In this study, the power consumption values for each considered system realisation were evaluated using different cross-channel intervals on the ground that cross-channel interference is unique for each signal type, operating at the same frequency plan. Therefore it is not reasonable to analyse different systems using equal channel distribution if the purpose is to evaluate regeneration impact on the power efficiency and total power consumption. Lower frequency slot limit intended for analysis was chosen based on the highest spectral efficiency, which could be achieved guaranteeing the fulfilment of BER requirement. The upper limit was derived from conditions when the transmission reach attained its maximum, which meant that further increment of frequency slot would lead only to the minimisation of spectral efficiency without profitable impact on power consumption.

Since the present research considers different spectral efficiencies at different frequency slots, the transmission reach became a function of channel spacing. Relation between frequency slots, spectral efficiency (SE) and transmission reach is summarised in Table 3.

Table 3

Spectral Efficiency and System Reach at Different Channel Spacing Values

Channel Spacing (GHz)	SE (bit/Hz)	Reach (km)
10 Gbps NRZ-OOK		
12.50	0.80	160
18.75	0.53	1680
25.00	0.40	5700
31.25	0.32	8720
40 Gbps NRZ-DPSK		
50.00	0.80	160
56.25	0.71	240
62.50	0.64	560
75.00	0.53	960
87.50	0.46	1440
100.00	0.40	2080
112.50	0.36	2080
100 Gbps DP-QPSK		
31.25	3.20	160
37.50	2.67	400
43.75	2.29	1040
50.00	2.00	1360

By defining transmission reach of the system and power consumption of WDM elements, the power efficiency and power ratio of 3R regenerators were evaluated. The results are shown in Figs. 1–6.

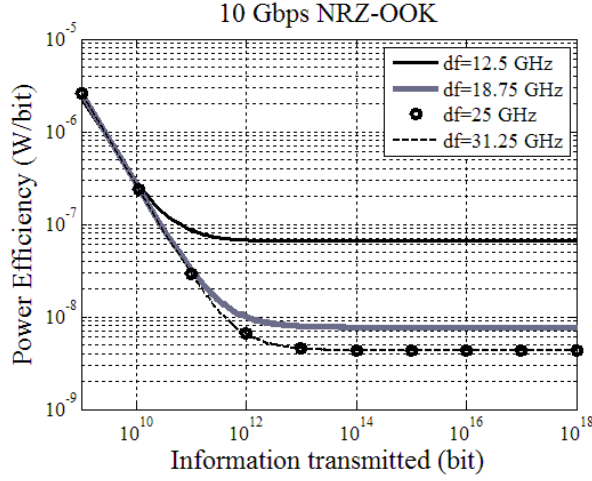


Fig.1. 10 Gbps NRZ-OOK power efficiency curve.

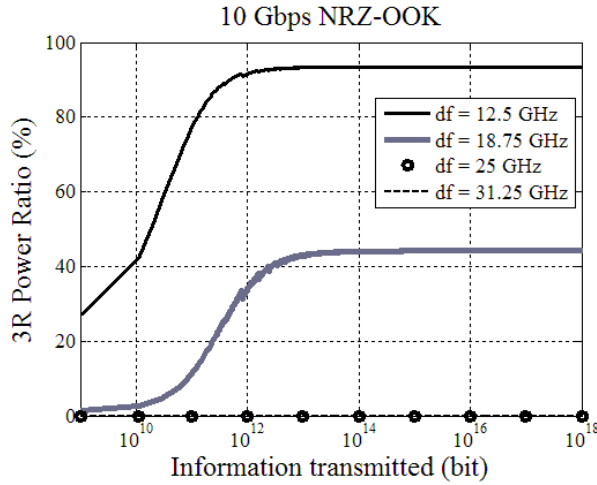


Fig.2. Power ratio curve of 10 Gbps NRZ-OOK 3R regenerators.

Figures 1–2 show the curves of the considered parameters for 10 Gbps NRZ-OOK system configuration from which it can be observed that when the total transmitted traffic reaches $\approx 10^{13}$ bits, power efficiency and 3Rs consumed power ratio stabilise, which allows making an assumption that parameters will not significantly change during system functioning and the obtained values can be used for system assessment and comparison. In spite of equal power efficiency, operation on the channel spacing values greater than 25 GHz in the considered system is impractical in terms of spectral efficiency. Signal reach in those cases become greater than transmission span and signal regeneration is not required, thus power efficiency reaches minimal value in this instance – 4.30 nW/bit. In the case of 12.5 GHz and 18.75 GHz

frequency slots, PE values are 7.7 and 65.5 nW/bit, respectively, which is a relatively abrupt leap of power consumption because for the transmission of a single bit the energy required is more than 15 times greater than using 25 GHz frequency span. Thus, it can be concluded that if spectral efficiency should be increased, other signal types should be considered possibly better solutions from the power consumption point of view, because as it can be seen from Fig. 2, using 12.5 GHz and 18.75 GHz frequency slots between channels, 10 Gbps signal regeneration requires 93.43 % and 44.15 % of total power consumed, respectively.

The second transmission signal type under consideration was 40 Gbps NRZ-DPSK. Figures 3–4 and Table 3 show spacing values of the considered channel. Since in this case transmission speed was 40 Gbps, signal spectrum was considerably wider in comparison with 10 Gbps NRZ-OOK spectra. This led to wider frequency slot requirement with the purpose to achieve the same quality of transmission (QoT) and thus the systems were evaluated using 50.0–100.0 GHz channel spacing. Six cross-channel intervals were analysed. The obtained results are provided in Table 4.

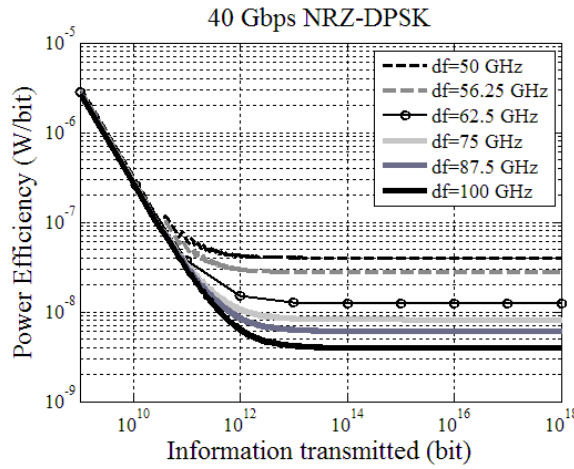


Fig.3. 40 Gbps NRZ-DPSK power efficiency curve.

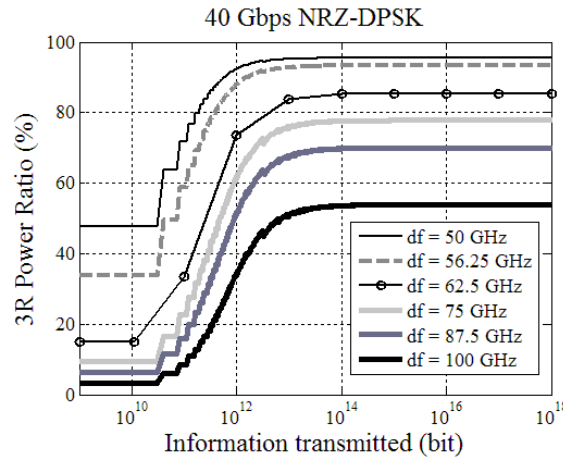


Fig. 4. Power ratio curve of 40 Gbps NRZ-DPSK 3R regenerators.

Table 4

Power Ratio Values of PE and 3Rs Operating at Different Frequency Slots

Channel spacing (GHz)	Power efficiency (nW/bit)	Power ratio of 3Rs (%)
50.00	40.07	95.46
56.25	27.32	93.34
62.50	12.44	85.38
75.00	8.19	77.80
87.50	6.07	70.03
100.00	3.94	53.88

On the ground of wider signal spectrum, by increment of frequency slot the power efficiency changed smoother than in the case of 10 Gbps. Therefore, increment of channel spacing for the amount of 12.5 GHz had no such significant impact on the power efficiency of the system. In this case, the power ratio of 3Rs had more significant impact on total power consumption (more than 50 % for each considered configuration) in comparison with NRZ-OOK because the transmission reach for this signal type was shorter. However, if 40 Gbps NRZ-DPSK operates with 100.0 GHz channel spacing, its power efficiency value is 3.94 nW/bit, when the best scenario for 10 Gbps NRZ-OOK is 4.3 nW/bit operating with 25.0 GHz frequency slot. This means that for the transmission of a single bit NRZ-OOK consumes by ≈ 8.37 % more power than NRZ-DPSK having the same spectral efficiency.

A similar situation occurs in scenarios when cross-channel interference is most pronounced, operating with 12.5 and 50.0 GHz channel spacing, respectively. In spite of the fact that power ratio of 3Rs for OOK and DPSK is 93.43 % and 95.46 % respectively, power efficiency at 40 Gbps system realisation is 40.07 nW/bit against 65.5 nW/bit in the case of 10 Gbps, which provides ≈ 63 % difference in the required power for the transmission of a single bit.

The results of 100 Gbps DP-QPSK are summarised in Figs. 5–6.

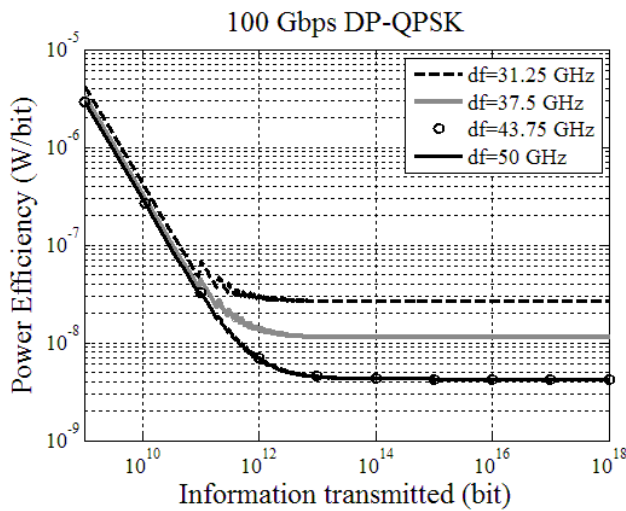


Fig. 5. 100 Gbps DP-QPSK power efficiency curve.

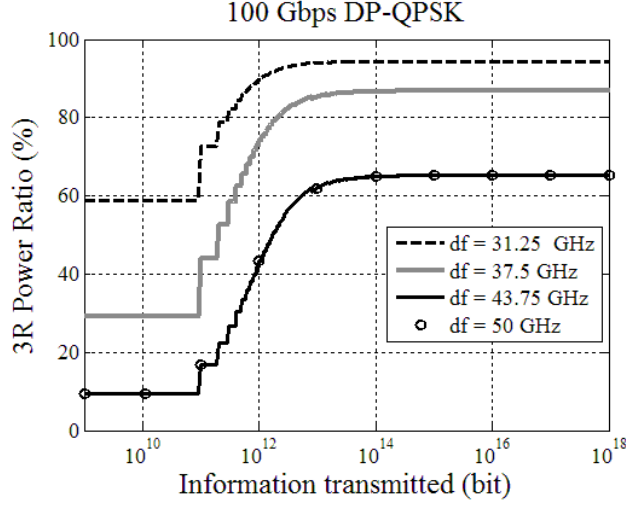


Fig. 6. 100 Gbps DP-QPSK 3R power ratio curve.

The obtained results show that minimal channel spacing to guarantee the required BER level is 31.25 GHz, which provides the power efficiency level equal to 26.50 nW/bit. In virtue of a very efficient modulation format, spectral efficiency in this case is four times greater in comparison with both 10 Gbps NRZ-OOK and 40 Gbps NRZ-DPSK and, furthermore, the considered transmission system is power efficient by 147 % and 51 % in comparison with NRZ-DPSK and NRZ-OOK, respectively. Other issues are practical and financial realisations of such signal transmittance, but this is out of scope of the present research.

Likewise in the previous instances, signal regeneration requires great amount of energy, even when cross-channel interference becomes minimal and only one regeneration action is required. In this case, 3Rs ratios are 65.26 %, 86.80% and 94.42% operating at 43.75, 37.5 and 31.25 GHz cross-channel intervals, respectively. Investigation has shown that using channel spacing values greater than 43.75 GHz for the considered system is unreasonable and does not have impact on the power consumption of the system. Using 43.75 GHz cross-channel intervals, the power efficiency parameter of the system is 4.26 nW/bit, which means that 40 Gbps NRZ-DPSK transmission system, which uses 100 GHz frequency spans, can be by ≈ 8.1 % more power efficient than 100 Gbps DP-QPSK in the best scenario.

4. CONCLUSIONS

In the present research, the power efficiency of the three most popular signal modulation formats in the long-haul DWDM systems has been studied. The analytic model has been designed with the purpose that the error probability ratio for signal detection should be maintained lower than 10^{-3} at the receiving node at 2960 km P2P transmission distance. For this purpose by means of simulation using OptSim software, the transmission reach for each setup has been defined and using the obtained results the power consumption and efficiency of the system have been calculated. In addition, the impact of signal regeneration procedure has been examined on the total

power consumption of the system for each simulation setup. The evaluation results have been presented as the functions of transmitted data volume operating at different channel spacing values, which allows adapting the results for WDM realisations with different available spectral bands.

The present research provides power efficiency values and the comparison for the DWDM setups, which operate with 10 Gbps NRZ-OOK, 40 Gbps NRZ-DPSK or 100 Gbps DP-QPSK transmission signals, and gives an insight into the required power ratio intended for the considered signal regeneration. The results obtained within the framework of the research for the mentioned setups can provide useful guidance on designing a power-efficient DWDM long-haul system.

REFERENCES

1. Iyer, S., & Singh, S.P. (2016). Spectral and power efficiency investigation in single- and multi-line-rate optical wavelength division multiplexed (WDM) networks. *Photonics Network Communications*. doi:10.1007/s11107-016-0618-3
2. Keiser, G. E. (1998). A review of WDM technology and applications. *GTE Systems & Technology*, 21.
3. Pavlovs, D., Grinčišins, A., Bobrovs, V., Gavars, P., & Ivanovs, Ģ. (2016). Research of 10 Gbps NRZ-OOK signal spectral and energy efficiency. In *Proc. ELECTRONICS 2016*, 13 – 15 June 2016 (pp. 25–29). Lithuania: Kaunas University of Technology.
4. Pavlovs, D., & Bobrovs, V. (2016). Relationship between spectral efficiency and energy efficiency in 10 Gbps NRZ-OOK, 40 Gbps NRZ-DPSK and 100 Gbps DP-QPSK WDM transmission systems. In *Progress in Electromagnetic Research Symposium (PIERS 2016)*, 8–11 August 2016 (pp.1434–1438). Shanghai, China. doi:10.1109/PIERS.2016.7734673
5. Haykin, S., & Moher, M. (2007). *An introduction to analog and digital communications*. John Wiley & Sons.
6. Morea, A., & Spadaro, S., Rival, O., Perelló, J., Agraz, F., & Verchere, D. (2011). *Power Management of Optoelectronic Interfaces for Dynamic Optical Networks*. DOI: 10.1364/ECOC.2011.We.8.K.3
7. Chiani, M., Win, M. Z., & Zanella, A. (2003). Error probability for optimum combining of M-ary PSK signals in the presence of interference and noise. *IEEE Transactions On Communications*, 51(11). doi: 10.1109/TCOMM.2003.819197
8. Meghdadi, V. (2008). *BER calculation*. Wireless Communications by Andrea Goldsmith.
9. Van Heddeghem, W., Idzikowski, F., Vereecken, W., Colle, D., Pickavet, M., & Demeester, P. (2012). Power consumption modeling in optical multilayer networks. *Photonics Network Communications*, 24(2), 86–102. doi:10.1007/s11107-011-0370-7
10. Verbrugge, S., Colle, D., Demeester, P., Huelsermann, R., & Jaeger, M. (2005). General availability model for multilayer transport networks. In *Proc. 5th International Workshop on Design of Reliable Communication Networks*, 16–19 October 2005. Lacco Ameno, Island of Ischia, Italy. DOI: 10.1109/DRCN.2005.1563848

SIGNĀLA REĢENERĀCIJAS IETEKMES NOVĒRTĒŠANA UZ GARĀS DWDM SISTĒMAS ENERGOEFEKTIVITĀTI

D. Pavlovs, Vj. Bobrovs, M. Parfjonovs, A. Alševska, Ģ. Ivanovs

Kopsavilkums

Šajā rakstā ir izpētīta DWDM sistēmu energoefektivitātes lieluma atkarība no izvēlēta pārraides frekvences plāna, kurš izveidots saskaņā ar ITU-T rekomendāciju G.694.1. Ir aprēķināti reģenerācijas iecirkņa garumi un spektrālās efektivitātes lielumi, izmantojot dažādus starpkanālu intervālus. Atsevišķi rakstā ir analizēta signālu reģenerācijas procedūrai nepieciešamā jauda, kura ir grafiski attēlota kā attiecība pret sistēmas kopējo patērēto jaudu. Visi aprēķini tika izpildīti trim populārākajiem signālu modulācijas formātiem - NRZ-OOK, NRZ-DPSK un DP-QPSK, ar 10 Gbps, 40 Gbps un 100 Gbps pārraides ātrumiem attiecīgi, kuri bieži tiek izmantoti mūsdienīgās DWDM sistēmās. Rezultāti ir attēloti kā funkcijas no pārraidītās informācijas apjoma, kas padara tos piemērotām sistēmām ar atšķirīgu pieejamu spektra platumu.

17.08.2017.

